

SUPER HARDENING OF W/NbN NANOLAYERS UNDER SHALLOW
NANOINDENTATION

by

Brian Michael Ennis

BSME, University of Pittsburgh, 2002

Submitted to the Graduate Faculty of

School of Engineering in partial fulfillment

of the requirements for the degree of

Master of Science Mechanical Engineering

University of Pittsburgh

2002

UNIVERSITY OF PITTSBURGH

School of Engineering

This thesis was presented

by

Brian Michael Ennis

It was defended on

August 19, 2002

and approved by

Dr. William S. Slaughter, Associate Professor, Dept. of Mechanical Engineering

Dr. Michael R. Lovell, Associate Professor, Dept. of Mechanical Engineering

Thesis Advisor: Dr. Scott X. Mao, Professor, Dept. of Mechanical Engineering

ABSTRACT

SUPER HARDENING OF W/NbN NANOLAYERS UNDER SHALLOW NANOINDENTATION

Brian Michael Ennis, M.S.

University of Pittsburgh, 2002

Superlattice materials are nanocomposites that exhibit a hardness at small bilayer repeat periods which exceeds the hardness predicted by the rule of mixtures for composites. The objective of this investigation was to utilize the experimental data obtained from nanoindentations and image scanning to examine the behavior of the superlattice material, W/NbN. Nanoindentations and *in situ* surface imaging were conducted over a range of applied loads on samples of W/NbN with two different bilayer periods ($\Lambda=5.6$ nm and $\Lambda=10.4$ nm), and monolithic samples of the niobium nitride (NbN) ceramic and the tungsten (W) metal which comprise the superlattice material. Additional shallow nanoindentations were made to a depth equal to the individual layer thicknesses of the nanocomposites. The mechanical properties were determined using the Oliver and Pharr method and compared for all the samples. The load versus displacement curves were also compared. The energies of indentation were calculated. The characteristics of the material pile-up resulting from the nanoindentations are determined from the scanned surface images. The experimental results are discussed to evaluate the influence of the different factors to the increase in hardness. The results indicate that the elastic modulus does not influence the hardness of the superlattice materials. The hardness and load versus displacement curves for the shallow indentations show little difference in behavior between NbN sample and the two superlattice materials. However, an increase in hardness is observed in the

superlattice materials at deeper indentation depths. The results indicate that this increase in hardness is related to the nature of the interface between the layers in the superlattice materials.

TABLE OF CONTENTS

ABSTRACT.....	iii
LIST OF TABLES.....	vi
LIST OF FIGURES.....	vii
1.0 INTRODUCTION.....	1
2.0 BACKGROUND.....	4
2.1 Sample Preparation.....	4
2.2 Sample Structure.....	4
3.0 EXPERIMENTAL PROCEDURE.....	7
4.0 EXPERIMENTAL RESULTS.....	25
4.1 Hardness.....	26
4.2 Elastic Moduli.....	30
4.3 Load vs. Displacement Curves.....	32
4.4 Elastic / Plastic Energy of Indentation.....	40
4.5 Material Pile-Up.....	44
5.0 DISCUSSION.....	51
6.0 CONCLUSIONS.....	55
BIBLIOGRAPHY.....	57

LIST OF TABLES

Table 1: General property data of W/NbN samples.....	5
Table 2: General property data for W and NbN samples.....	5
Table 3: Summary of applied loads used for deep indentations.	13
Table 4: Summary of applied loads used for shallow indentations.	14
Table 5: Surface roughness statistics of each sample (for shallow indentations only).....	16
Table 6: Summary statistics for Reduced Moduli.....	31

LIST OF FIGURES

Figure 1: Structure and composition of samples used for experimentation - (a) thru (d).....	6
Figure 2: Schematic representation of the nanoindentation/scanning system.	7
Figure 3: SEM image of one of the 90° indenter tips used for nanoindentation.	8
Figure 4: Definition of terms using a typical load versus displacement curve.	9
Figure 5: Typical Roughness Analysis used to determine the surface roughness.	15
Figure 6: 3-D surface topography for NbN sample (pre-indentation).	17
Figure 7: Typical section of surface for NbN sample (pre-indentation).....	17
Figure 8: 3-D surface topography for NbN sample (post-indentation).....	18
Figure 9: Typical section of surface for NbN sample (post-indentation).	18
Figure 10: 3-D surface topography for W sample (pre-indentation).	19
Figure 11: Typical section of surface for W sample (pre-indentation).....	19
Figure 12: 3-D surface topography for W sample (post-indentation).....	20
Figure 13: Typical section of surface for W sample (post-indentation).	20
Figure 14: 3-D surface topography for W/NbN ($\Lambda=5.6$ nm) sample (pre-indentation).	21
Figure 15: Typical section of surface for W/NbN ($\Lambda=5.6$ nm) sample (pre-indentation).	21
Figure 16: 3-D surface topography for W/NbN ($\Lambda=5.6$ nm) sample (post-indentation).	22
Figure 17: Typical section of surface for W/NbN ($\Lambda=5.6$ nm) sample (post-indentation).	22
Figure 18: 3-D surface topography for W/NbN ($\Lambda=10.4$ nm) sample (pre-indentation).	23

Figure 19: Typical section of surface for W/NbN ($\Lambda=10.4$ nm) sample (pre-indentation).	23
Figure 20: 3-D surface topography for W/NbN ($\Lambda=10.4$ nm) sample (post-indentation).	24
Figure 21: Typical section of surface for W/NbN ($\Lambda=10.4$ nm) sample (post-indentation).	24
Figure 22: Hardness as a function of maximum indentation depth (Stage 1 indentations).	26
Figure 23: Hardness as a function of maximum indentation depth (Stage 2 indentations).	28
Figure 24: Comparison of the reduced modulus for each sample.	30
Figure 25: Comparison of load vs. displacement data for W/NbN ($\Lambda=5.6$ nm) sample.	32
Figure 26: Comparison of load vs. displacement data for W/NbN ($\Lambda=10.4$ nm) sample.	33
Figure 27: Comparison of load vs. displacement data for same indentation depth.	34
Figure 28: Comparison of load vs. displacement data for same load.	35
Figure 29: Comparison of load vs. displacement data for final indentation depth of 3 nm.	36
Figure 30: Comparison of load vs. displacement data for final indentation depth of 8 nm.	36
Figure 31: Comparison of load vs. displacement data for final indentation depth of 13 nm.	37
Figure 32: Comparison of load vs. displacement data for final indentation depth of 110 nm.	37
Figure 33: Ratio (h_f / h_{max}) as a function of maximum indentation depth.	39
Figure 34: Definitions for energy of indentation.	40
Figure 35: Comparison of the total energy of indentation as a function of h_f	41
Figure 37: Comparison of the plastic energy of indentation as a function of h_f	42
Figure 39: Comparison of pile-up for samples (a) thru (d) for same final indentation depth.	44
Figure 40: Definitions of pile-up terminology.	45
Figure 41: Sections used for pile-up analysis.	46
Figure 42: Pile-up Height, t , as a function of maximum indentation depth.	47
Figure 43: Ratio (a/t) as a function of maximum indentation depth, h_{max}	47

Figure 44: Ratio (c/t) as a function of maximum indentation depth, h_{\max}	48
Figure 45: Pile-up Height, t , as a function of final indentation depth, h_f	48
Figure 46: Ratio (a/t) as a function of final indentation depth, h_f	49
Figure 47: Ratio (c/t) as a function of final indentation depth, h_f	49
Figure 48: Cracking in the ceramic sample, NbN.....	53
Figure 49: Bending of the nanolayers in the nanocomposites.....	54

1.0 INTRODUCTION

Superlattice materials are nanocomposites formed by depositing alternating layers of different material composition that are typically only a few nanometers thick. The primary interest in these materials has been due to an experimentally observed hardness which is greater than the theoretical hardness predicted by the rule of mixtures for normal composites. As a result, these materials have been investigated for possible use as thin film coatings to improve wear resistance. As manufacturing techniques improve and the demand for specialized material coatings increases, the need to quantify and understand the strengthening and deformation mechanisms operating in this class of materials becomes more important so as to provide a means to evaluate and optimize their use for specific engineering applications

Multilayered materials have been the focus of a significant amount of research. Madan and Barnett [1,2] have explored several different types of nitride based superlattice thin films and have described the fabrication, the structure and the hardness behavior of various thin films. Chu, Wong, Sproul and Barnett [3] examined polycrystalline transition metal nitride superlattice films and demonstrated that the hardness for several materials is inversely proportional to the bilayer repeat period and showed that there is an optimum bilayer repeat period that maximizes the hardness for some materials. They also discussed several possible explanations for the hardness behavior such as the supermodulus effect, coherency strains, grain size reduction and Koehler's model. Clemens, Kung and Barnett [4] reviewed the hardness of several metallic and superlattice

materials and discussed the strain relaxation, interface morphology and Koehler's model. Anderson, Foecke and Hazzledine [5] examined 50 vol% Cu-50 vol% Ni multilayered samples and discussed the propagation of dislocation loops confined between the layers and the nucleation of dislocations at the interface. Thus, different classes of multilayered materials have been examined, and several theories have been proposed to explain the mechanisms that may operate to produce this increase in hardness in these materials: the supermodulus effect, coherency strains, the effect of interfacial misfit dislocations on dislocation glide, the reduction of grain sizes as a result of thickness of the alternating layers, and image forces (Koehler's model) at the interface which resist dislocation glide. [3, 4] However, while these articles describe the properties of different types of superlattice materials, most of the studies have focused on the fabrication of these materials and the relationship between the hardness of the material and the bilayer repeat period (i.e. the total thickness of a single pair of the alternating layers). [1]

Nanoindentation is an experimental tool that has been used in different ways to investigate the properties of thin films and multilayered materials. Kramer, et al. [6] used nanoindentation to investigate the behavior of thin soft films on a hard substrate. Whittling, et al. [7] examined the deformation behavior of a TiN film on different substrates to evaluate the influence of the substrate on thin film behavior. Tymiak, et al. [8] explored the use of nanoindentation as a tool to evaluate the fracture toughness of bimaterial films. Tambwe, et al. [9] used the results of nanoindentation experiments to determine the composition of nanolayered materials. Hence, the innovative use of nanoindentation has proven to be an important tool for research conducted to increase the understanding of the behavior of multilayered materials and thin films.

To date, there has been no analysis of a superlattice material's behavior as a function of the indentation depth, and the role of the interface in the super hardening behavior observed in several multilayered materials. To study this phenomenon, shallow nanoindentations were conducted on two samples of the superlattice material W/NbN, each with a different bilayer repeat period ($\Lambda=5.6$ nm and $\Lambda=10.4$ nm), to indentation depths equal to the thickness of the individual layers. This unique use of nanoindentation examines the influence of the individual interfaces on material behavior. Additional nanoindentations were made at deeper indentation depths to complete the study. As Baker [10] and Gerberich, et al. [11] have discussed, the indenter tip shape and surface roughness of the sample can influence the experimental results obtained from nanoindentations. Consequently, the surface conditions of the samples prior to indentation are discussed for the shallow nanoindentations. The purpose of this investigation will be to compare the properties and behavior of the superlattice material with the properties and behavior of the two monolithic materials comprising the superlattice material as a function of the depth of indentation in order to analyze the deformation process of the nanolayers.

2.0 BACKGROUND

2.1 Sample Preparation

The superlattice material chosen for this investigation was W/NbN. [1, 2, & 12] Two samples of this nanocomposite were made for experimentation. Each superlattice material sample had a different bilayer repeat period, Λ : $\Lambda = 5.6$ nm for one sample and $\Lambda = 10.4$ nm for the other. This was done to evaluate the influence, if any, of the layer thickness on the results. These samples were fabricated by depositing alternating layers of single crystal tungsten (W) and niobium nitride (NbN) on a substrate. In addition, two other samples were made of each individual material used in the nanocomposite. All four samples were epitaxially grown as a thin film approximately 1 μm thick on an MgO $\langle 001 \rangle$ substrate using reactive DC magnetron sputtering. [13]

2.2 Sample Structure

The nanocomposite W/NbN is classified as an immiscible, non-isostructural superlattice material. This material is composed of alternating layers of a body-centered cubic metal (W) and a face-centered cubic ceramic (NbN). The ceramic layer has a lattice constant of 0.439 nm. The metal layer has a lattice constant of 0.315 nm. The structure of this material has been well documented in the literature. [1, 12] The lattice orientations, the microhardness, and the bilayer repeat period of each sample is listed in Table 1.

Table 1: General property data of W/NbN samples. [1, 12]

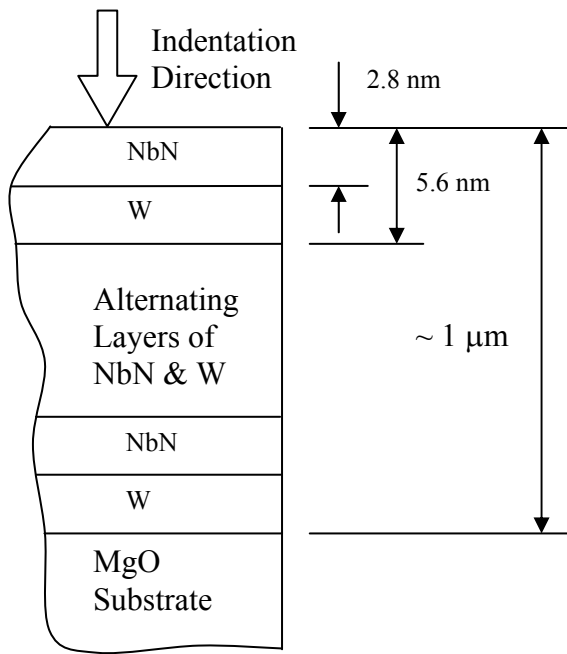
Sample	Bilayer Repeat Period (Λ)	Crystal Orientation	Microhardness
W/NbN ($\Lambda=5.6$ nm)	5.6 nm	(100) / (100)	28 GPa
W/NbN ($\Lambda=10.4$ nm)	10.4 nm	(100) / (100)	26 GPa

The NbN and W samples were fabricated using the same crystal structure and orientation as the thin layers used in the nanocomposites. Their mechanical properties are described in the literature and are listed in Table 2.

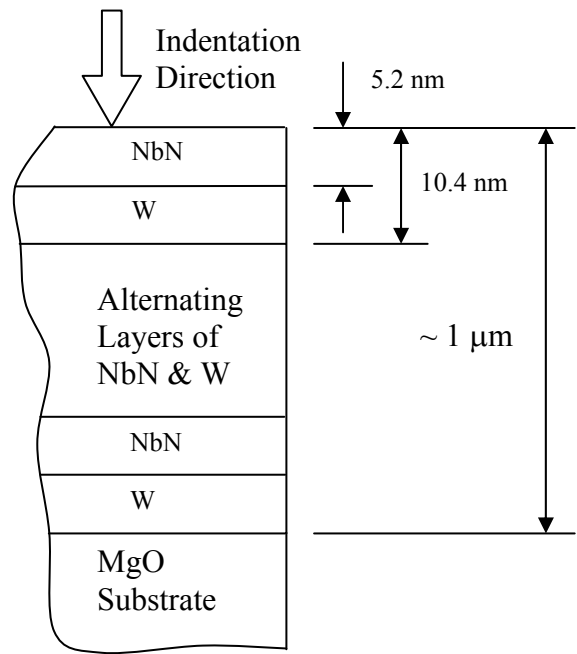
Table 2: General property data for W and NbN samples. [1, 3, 4, 14, 15]

Sample	Crystal Orientation	Microhardness	Young's Modulus	Shear Modulus	Poisson's Ratio
W	(100)	7 GPa	390-410	160	0.28
NbN	(100)	17 GPa	480-490	142	-

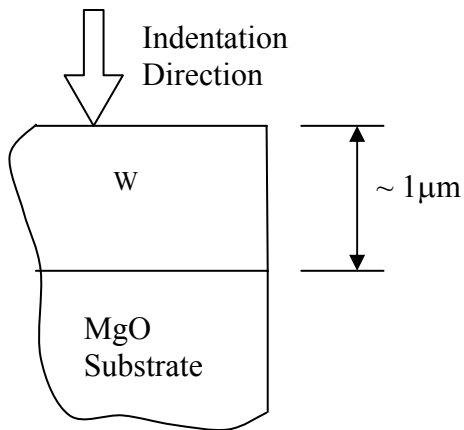
A pictorial representation detailing the composition of each sample is shown in Figure 1. Note that the ceramic, NbN, is the surface layer for both nanocomposite samples. [12]



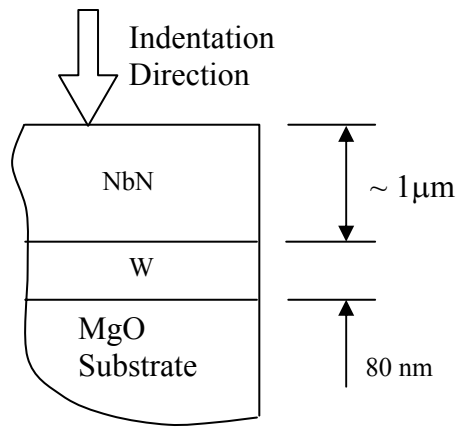
(a) Sample W/NbN($\Lambda=5.6$ nm)



(b) Sample W/NbN($\Lambda=10.4$ nm)



(c) W sample.



(d) NbN sample.

Figure 1: Structure and composition of samples used for experimentation - (a) thru (d). [12]

3.0 EXPERIMENTAL PROCEDURE

The experiments were conducted using Hysitron's Triboscope® Nanoindenter in conjunction with Digital Instruments' Nanoscope IIIa AFM imaging system. Each sample was ultrasonically cleaned with acetone to remove any surface debris. Prior to indentation, each sample was scanned to find suitable areas for indentation. The criteria used to evaluate the surface condition are explained in greater detail below. The Triboscope software was used to compensate for drift and the machine compliance during indentation. After indentation, the sample surface was scanned *in situ* to record the image of the surface topography. A schematic of the equipment is shown in Figure 2.

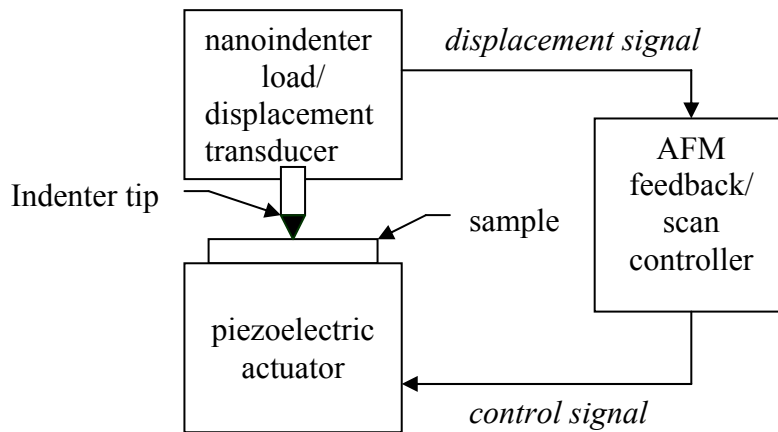


Figure 2: Schematic representation of the nanoindentation/scanning system.

Diamond cubic pyramidal indenter tips with an included angle of 90° were selected for the experiments since a sharp tip radius was necessary to achieve sufficient penetration into the hard samples. An image depicting the geometry of the cubic indenter tips used for the nanoindentation experiments is shown in Figure 3. The image was recorded using scanning electron microscopy (SEM).

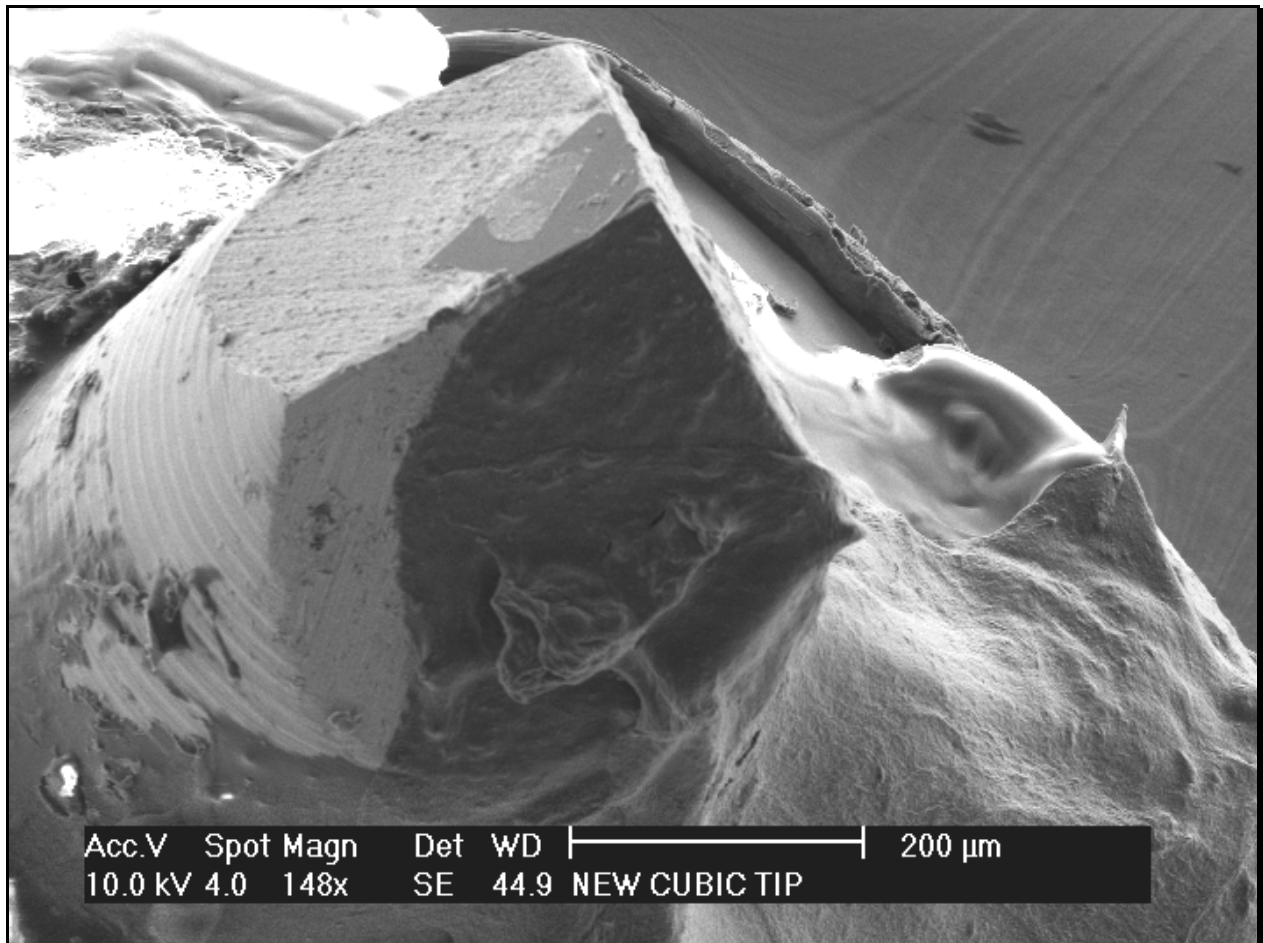


Figure 3: SEM image of one of the 90° indenter tips used for nanoindentation. [16]

For each indenter tip, nanoindentations were made on a standard fused quartz sample to determine the machine compliance and to calibrate the area functions. The machine compliance is the measure of the elongation of the machine in response to the applied load. Once the machine compliance is known, the software can compensate and eliminate its influence on the results. Oliver and Pharr [17] developed a method (which is summarized below) to determine two mechanical properties, the hardness and the elastic modulus, using the unloading portion of a load versus displacement curve. A typical curve defining the terminology is shown in Figure 4.

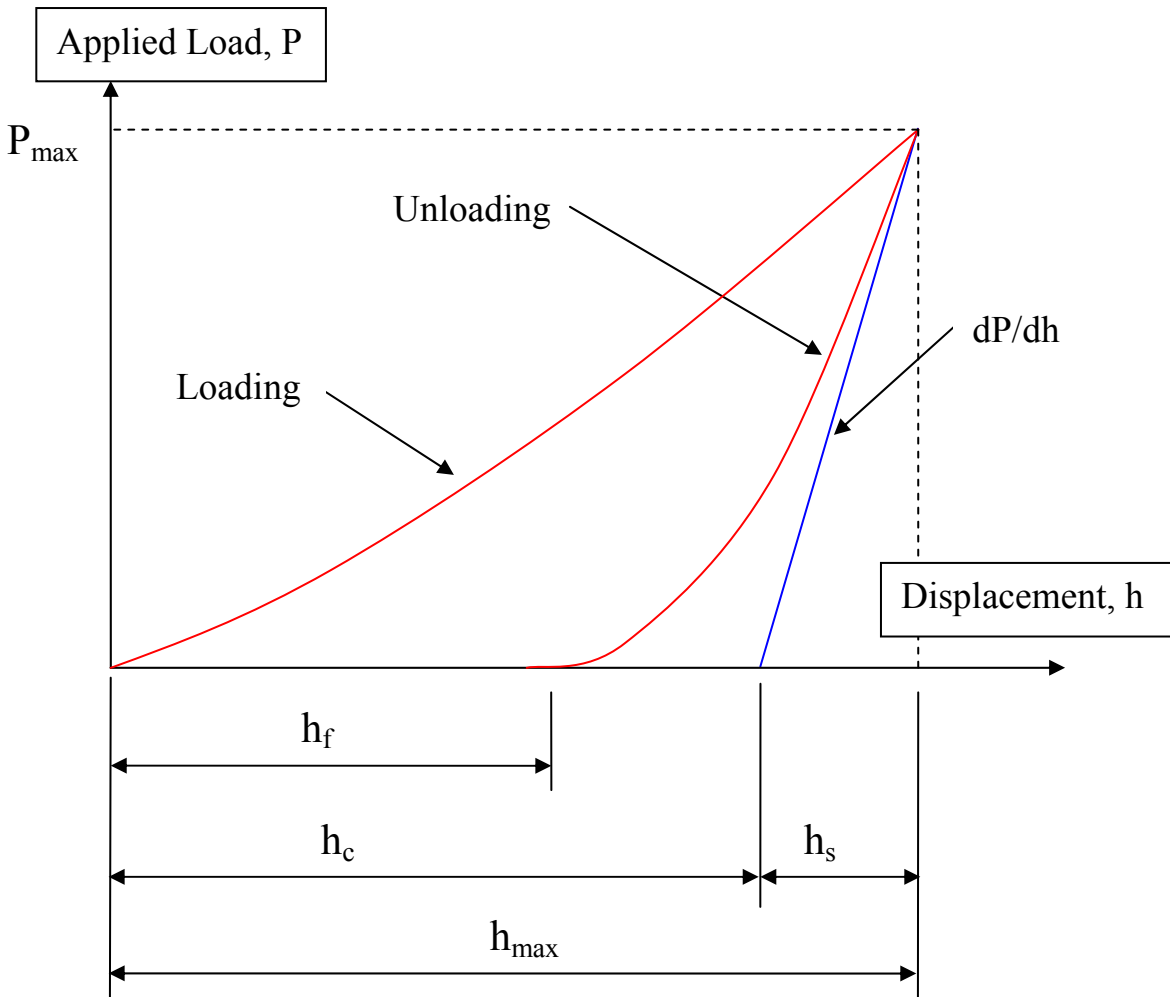


Figure 4: Definition of terms using a typical load versus displacement curve.

For nanoindentations, the hardness is normally defined as the maximum load divided by the projected area of the indenter in contact with the sample at the maximum load. Thus,

$$H = \frac{P_{MAX}}{A_C} \quad (1)$$

Where,

H = Hardness.

P_{MAX} = Maximum applied load.

A_C = Projected contact area at the maximum applied load.

Since the indenter tip is not rigid during indentation, the elastic modulus can not be directly determined from the load versus displacement curve. However, the reduced elastic modulus can be determined from the unloading portion of the curve by the relation [17]:

$$E_r = \frac{\sqrt{\pi}}{2} \cdot \frac{dP}{dh} \cdot \frac{1}{\sqrt{A_c}} \quad (2)$$

Where,

E_r = Reduced Modulus.

A_C = Projected contact area at the maximum applied load.

dP/dh = Experimentally measured stiffness.

The elastic modulus of the sample can then be calculated from the reduced modulus if the elastic modulus and Poisson's ratio of the indenter is known from the following equation [17]:

$$\frac{1}{E_r} = \left\{ \frac{(1-\nu^2)}{E} \right\}_{SPECIMEN} + \left\{ \frac{(1-\nu^2)}{E} \right\}_{INDENTER} \quad (3)$$

Where,

ν = Poisson's ratio.

E = Elastic Modulus.

E_r = Reduced Modulus.

The importance of determining the area function is evident from equations (2) and (3) since both the hardness and the reduced modulus are a function of it. The area functions were calculated by fitting the results of the nanoindentations to a polynomial of the form:

$$A_C = C_0 h_C^2 + C_1 h_C + C_2 h_C^{1/2} + C_3 h_C^{1/4} + C_4 h_C^{1/8} + C_5 h_C^{1/16} \quad (4)$$

Where,

A_C = Contact area as a function of the contact depth.

h_c = Contact depth of indenter at the maximum applied load.

C_0, C_1, C_2, C_3, C_4 & C_5 are constants.

The hardness and the reduced modulus are then calculated by substituting the contact area, determined from the area function based on the contact depth, into equations (2) and (3).

At first, the experiments were conducted by making three (3) indentations for each load applied to the sample. However, the results indicated that progressive wear of the indenter tip was occurring. This was due to the hardness of the materials being examined and the number of nanoindentations. Consequently, to prevent this factor from influencing the results, the number of nanoindentations was reduced to one (1) indentation per applied load to minimize the wear of the tip. Also, after conducting the nanoindentations on each sample, a few indentations were made at different loads on the standard quartz sample and compared to the calibration nanoindentations to confirm that the indenter geometry was not changing over the course of the experiment. The experiment was divided into two stages. The first stage, referred to as deep nanoindentations, examined the behavior of the materials as a function of the indentation depth. The second stage, referred to as shallow nanoindentations, examined the behavior of the materials at shallow indentation depths to evaluate the influence (if any) of the individual layers in the superlattice materials.

Stage 1: Deep Nanoindentation

In the first set of nanoindentations, the objective was to determine the variation of the hardness as a function of the indentation depth. To accomplish this task, nanoindentations were made at different loads ranging from 1000 μN to 9000 μN for the two nanocomposite samples of W/NbN, and from 500 μN to 9000 μN for the samples of W and NbN. A summary of the applied loads used for the deep indentations made on each sample is listed in Table 3. All the indentations were made at the same load rate of 100 μN per second to minimize any influence of the strain rate on the experiments. A 90° cubic pyramidal tip with a radius of approximately 90

nm was used. The surface areas varied from approximately 1 μm by 1 μm to 2 μm by 2 μm . The scan size was adjusted based on the anticipated size of the indenter contact area and the plastic zone radius. The surface height variation was required to be less than 10 nm over the entire scanned area to ensure a reasonably smooth and level surface for indentation.

Table 3: Summary of applied loads used for deep indentations.

W/NbN($\Lambda=5.6$ nm)		W/NbN($\Lambda=10.4$ nm)		NbN		W	
Applied Load	No. of Indents	Applied Load	No. of Indents	Applied Load	No. of Indents	Applied Load	No. of Indents
1000 μN	1	1000 μN	1	1500 μN	1	500 μN	1
2000 μN	1	2000 μN	1	2000 μN	1	750 μN	1
3000 μN	1	3000 μN	1	2500 μN	1	1000 μN	1
4000 μN	1	4000 μN	1	3000 μN	1	1500 μN	1
5000 μN	1	5000 μN	1	3500 μN	1	2000 μN	1
6000 μN	1	6000 μN	1	4000 μN	1	3000 μN	1
7000 μN	1	7000 μN	1	5000 μN	1	4000 μN	1
8000 μN	1	8000 μN	1	6000 μN	1	5000 μN	1
9000 μN	1	9000 μN	1	7000 μN	1	6000 μN	1
				8000 μN	1	7000 μN	1
				9000 μN	1	8000 μN	1
						9000 μN	1

Stage 2: Shallow Nanoindentation

In the second set of nanoindentations, the objective was to determine the effect (if any) that the individual layers have on the hardness of the nanocomposites. These shallow nanoindentations were restricted to achieve a penetration depth of less than 25 nm. For the superlattice material samples, the applied loads were selected to achieve penetration of the

indenter to a depth equal to the theoretical thickness of the individual layers of the material. The loads applied to the monolithic samples of W and NbN were chosen to match the depth of the penetrations into the superlattice materials as closely as possible. The applied loads used for the shallow indentations are listed in Table 4 for each sample. The indentations were made at the same load rate of 10 μN per second using a 90° cubic pyramidal tip with a 50 nm tip radius.

Table 4: Summary of applied loads used for shallow indentations.

W/NbN($\Lambda=5.6$ nm)		W/NbN($\Lambda=10.4$ nm)		NbN		W	
Applied Load	No. of Indents	Applied Load	No. of Indents	Applied Load	No. of Indents	Applied Load	No. of Indents
20 μN	1	65 μN	1	30 μN	1	25 μN	1
52 μN	1	80 μN	1	75 μN	1	60 μN	1
90 μN	1	135 μN	1	110 μN	1	90 μN	1
130 μN	1	180 μN	1	140 μN	1	110 μN	1
145 μN	1	250 μN	1	150 μN	1	125 μN	1
250 μN	1			210 μN	1	150 μN	1
				250 μN	1	160 μN	1
				300 μN	1	200 μN	1

As noted in the literature, the surface roughness of the sample can significantly influence the experimental results when conducting nanoindentation experiments. [10, 11] This is particularly important for shallow nanoindentations where the penetration of the indenter into the material is less than 25 nm. To minimize this influence, the sample surface was scanned *prior to* nanoindentation and the image was recorded. By doing this, the actual roughness of the surface area could be determined from this pre-indentation image utilizing the NanoScope IIIa software. An example of the screen displaying the results of the Roughness Analysis is shown in Figure 5.

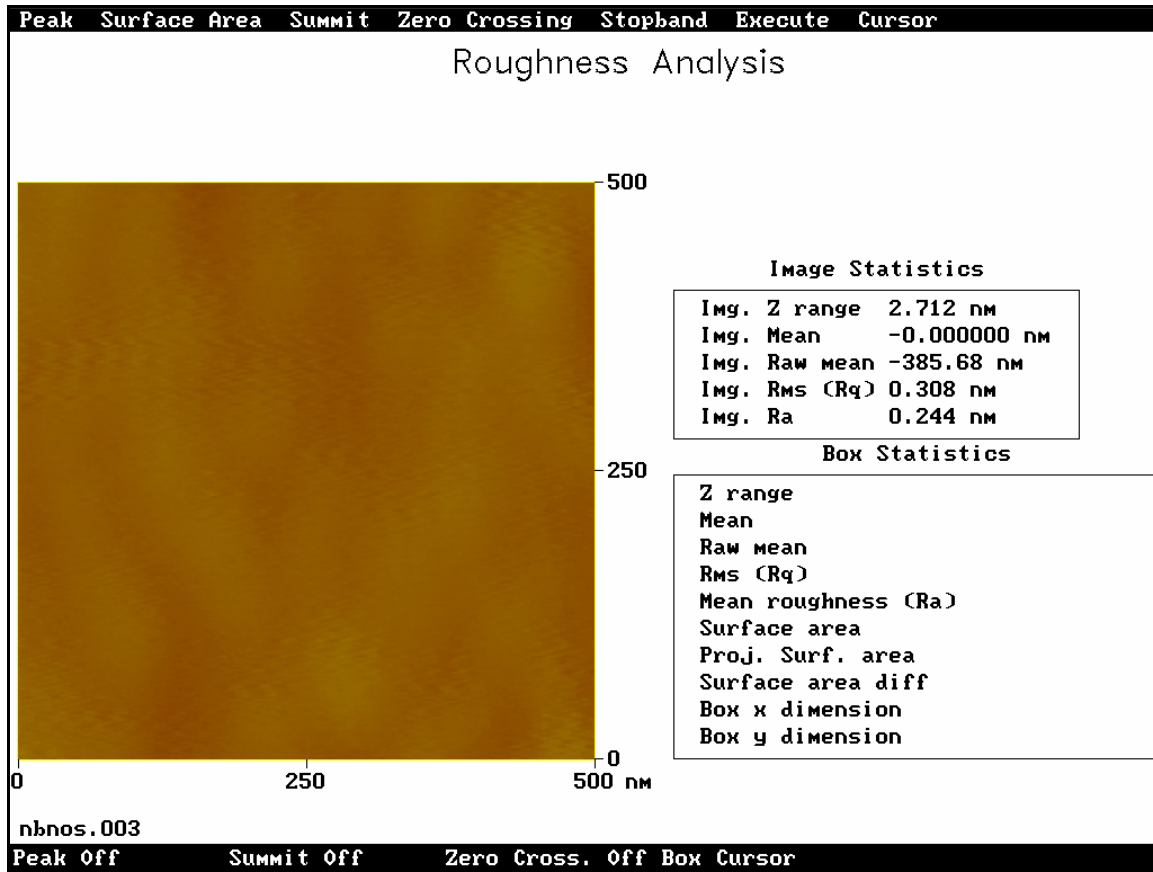


Figure 5: Typical Roughness Analysis used to determine the surface roughness.

The Roughness Analysis calculates two quantities, Ra and Rq (rms). The arithmetical average deviation, Ra, is the average of the absolute difference in height measured in the z-direction between a point and the reference plane. Rq is the root-mean-square average of the deviations in height. This quantity is determined by adding the squares of the deviations in the z-direction from the reference plane, by dividing by the number of data points examined, and finally taking the square root. Either quantity may be used to characterize the surface roughness of the sample. The Roughness Analysis was used to determine the surface roughness statistics for each sample. As shown in the results summarized in Table 5, the mean values of Ra and Rq (rms) were less than 0.5 nm for the scanned surface area of 500 nm by 500 nm.

Table 5: Surface roughness statistics of each sample (for shallow indentations only).

Material Sample	Rq (rms) Mean	Rq (rms) Std. Dev.	Ra Mean	Ra Std. Dev.
NbN	0.390 nm	0.076 nm	0.313 nm	0.066 nm
W	0.329 nm	0.200 nm	0.250 nm	0.152 nm
W/NbN ($\Lambda=5.6$ nm)	0.414 nm	0.017 nm	0.330 nm	0.017 nm
W/NbN ($\Lambda=10.4$ nm)	0.409 nm	0.014 nm	0.325 nm	0.013 nm

After indentation, the sample surfaces were also scanned. The surface topographies and cross sections of the pre-indentation and post-indentation images were then examined to verify that permanent deformation had occurred during the indentation. Examples of the pre-indentation and post-indentation 3-D surface topographies and section images for the shallow indentations are shown in Figures 6 through 20: see Figures 6-9 for images of the NbN sample, see Figures 10-13 for images of the W sample, see Figures 14-17 for images of the W/NbN ($\Lambda=5.6$ nm) sample, and see Figures 18-21 for images of the W/NbN ($\Lambda=10.4$ nm) sample.

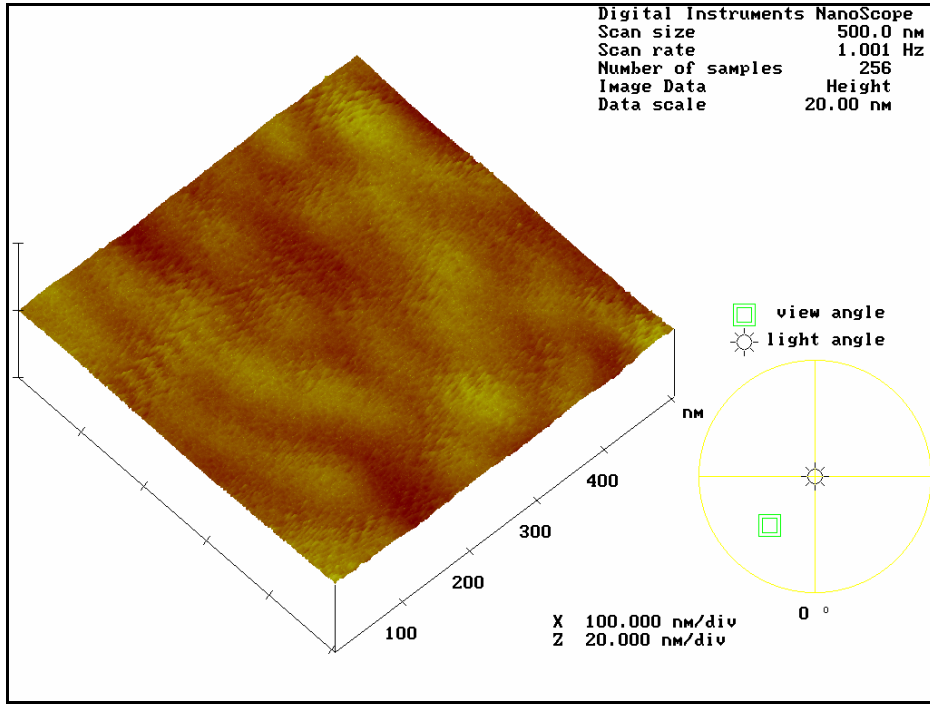


Figure 6: 3-D surface topography for NbN sample (pre-indentation).

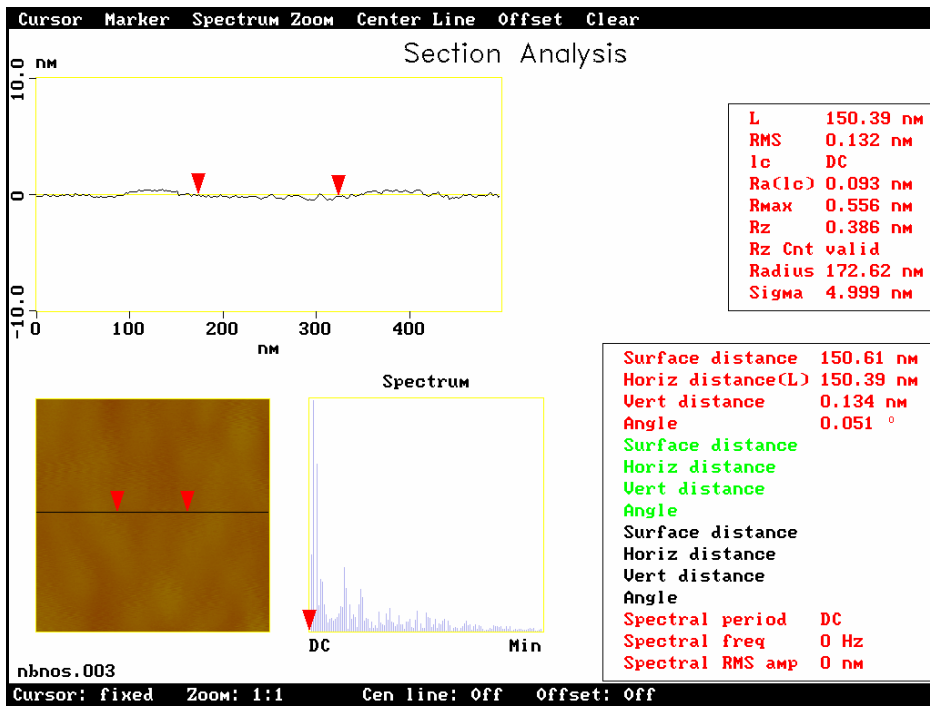


Figure 7: Typical section of surface for NbN sample (pre-indentation).

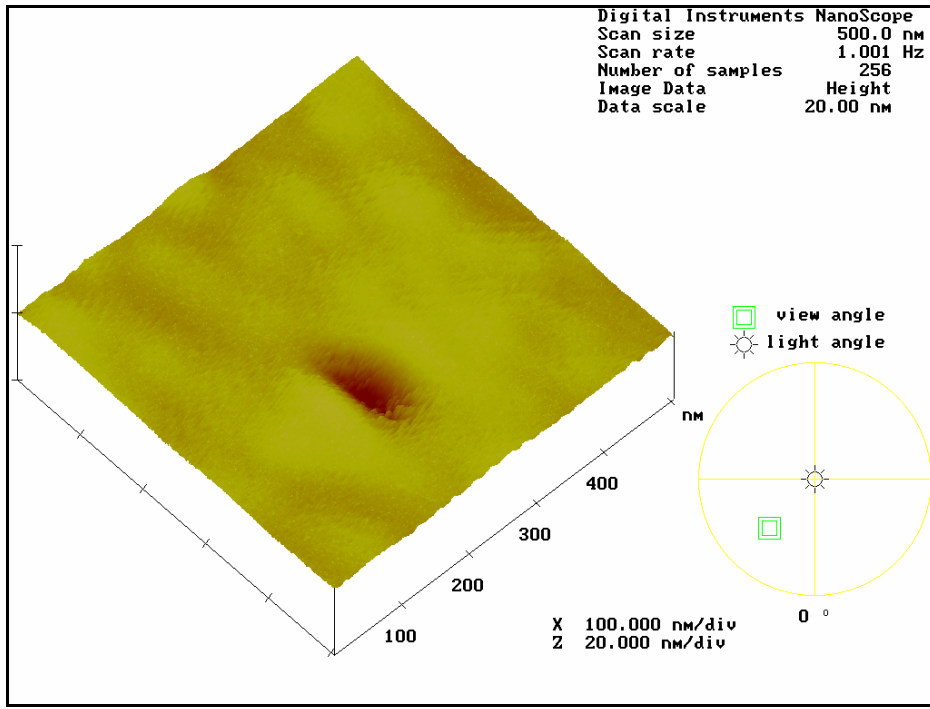


Figure 8: 3-D surface topography for NbN sample (post-indentation).

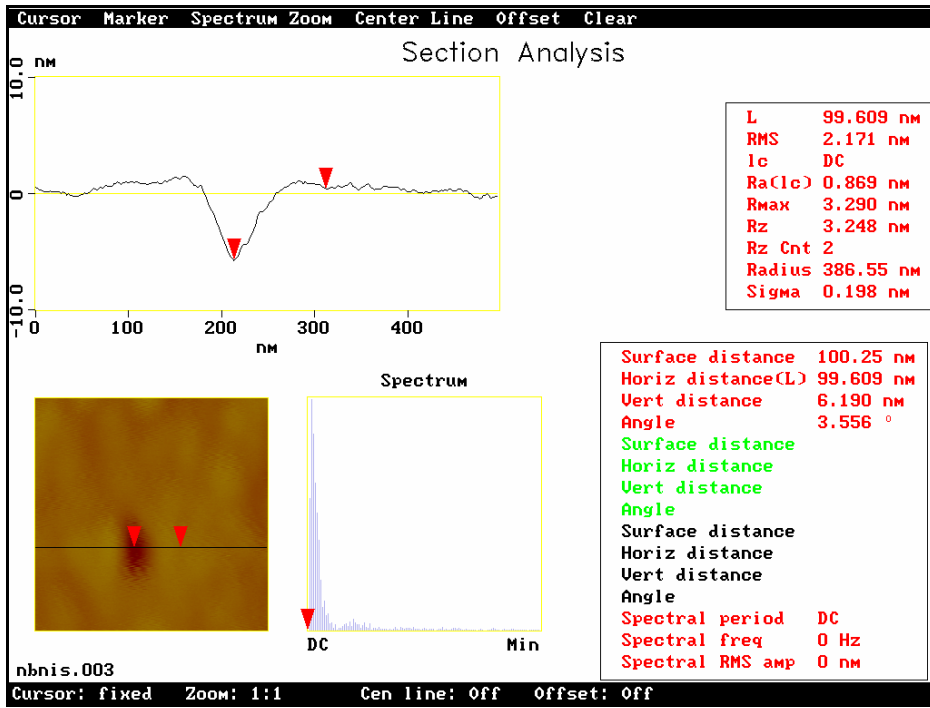


Figure 9: Typical section of surface for NbN sample (post-indentation).

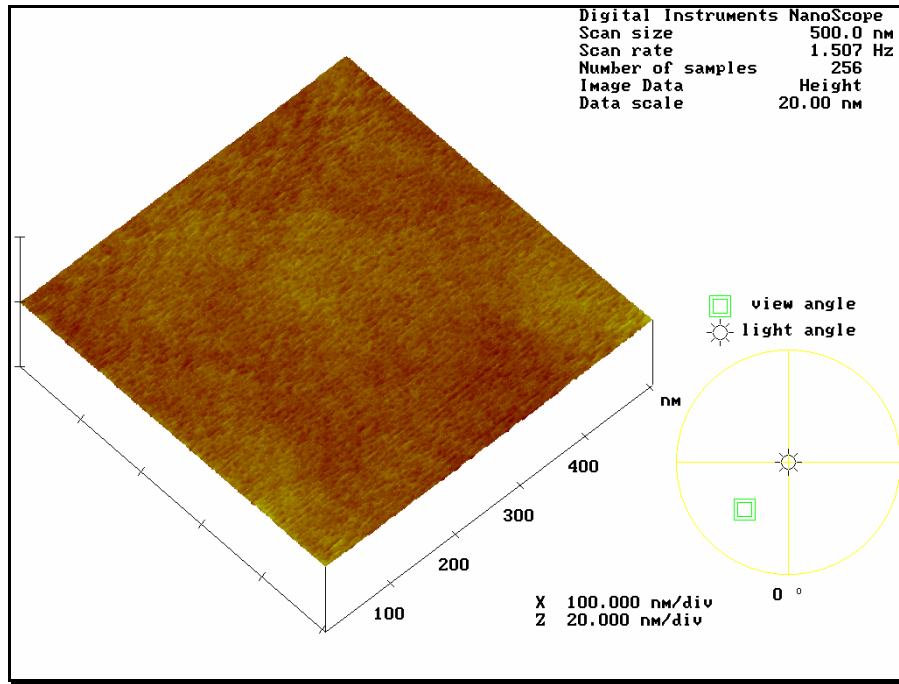


Figure 10: 3-D surface topography for W sample (pre-indentation).

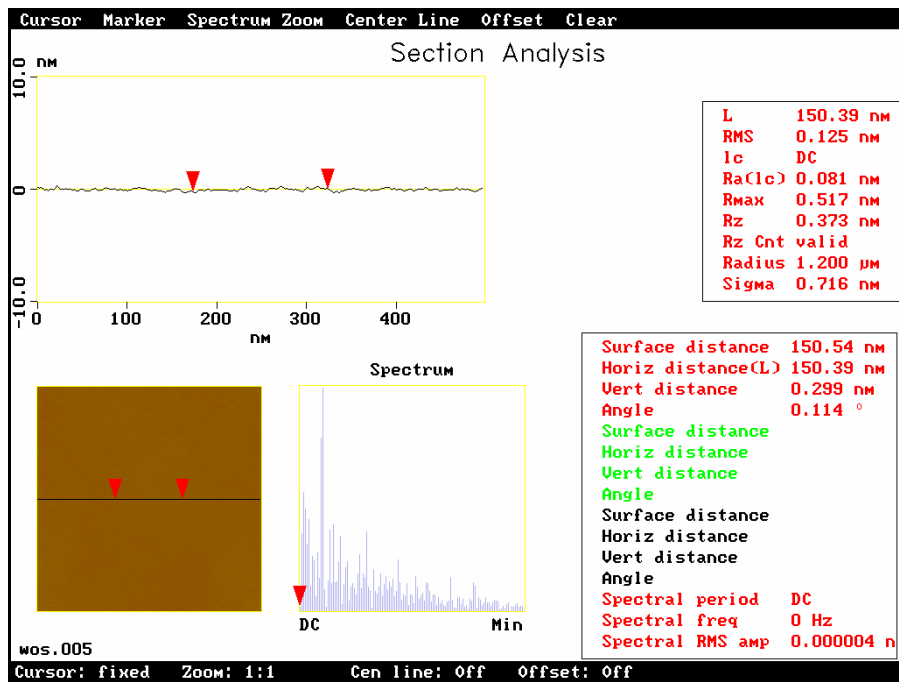


Figure 11: Typical section of surface for W sample (pre-indentation).

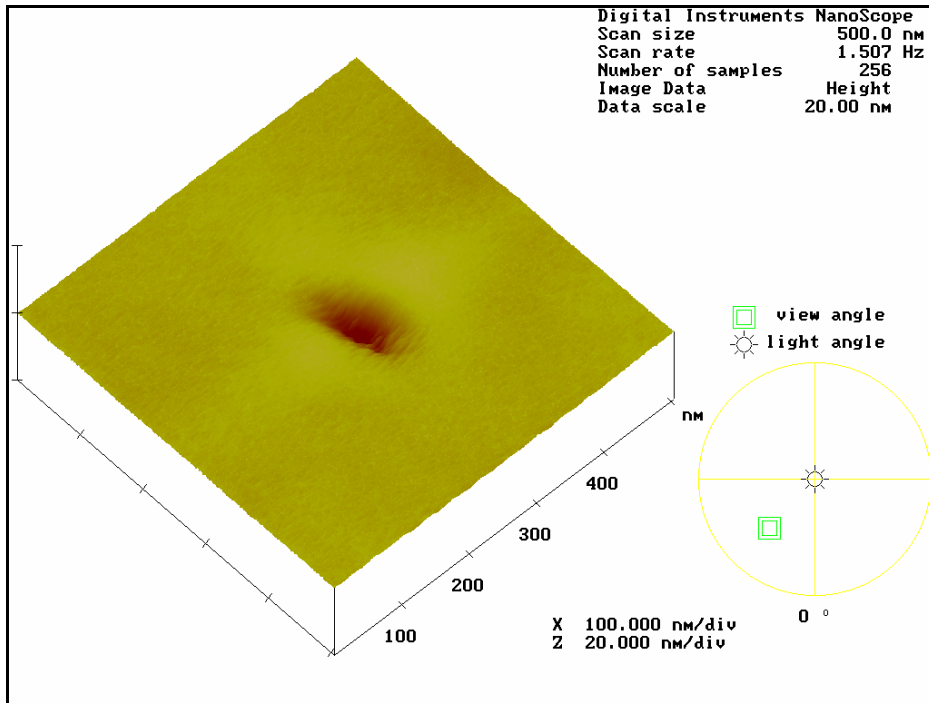


Figure 12: 3-D surface topography for W sample (post-indentation).

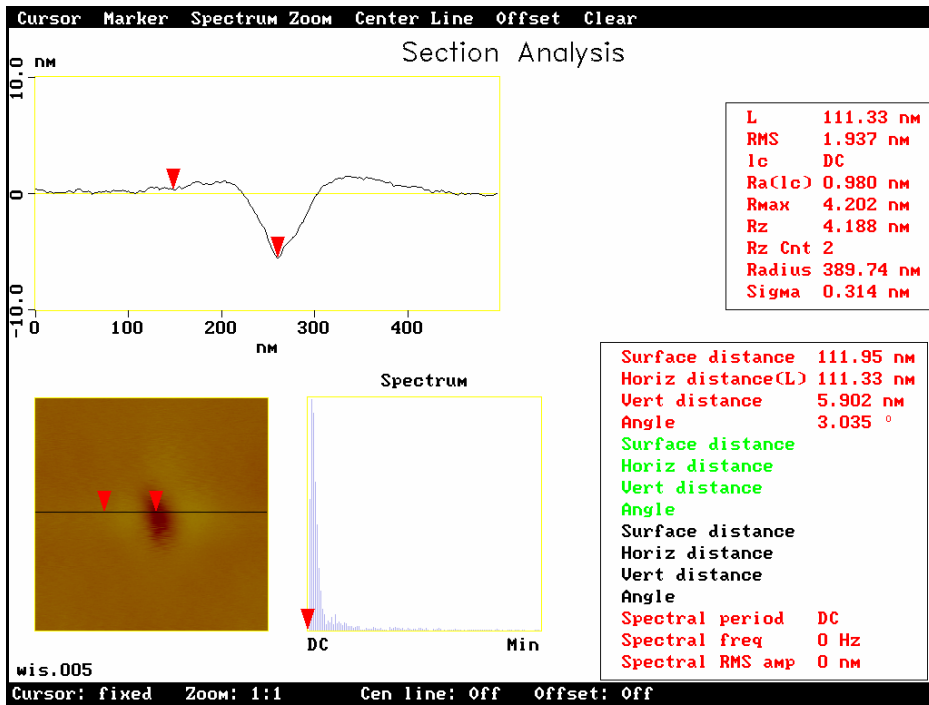


Figure 13: Typical section of surface for W sample (post-indentation).

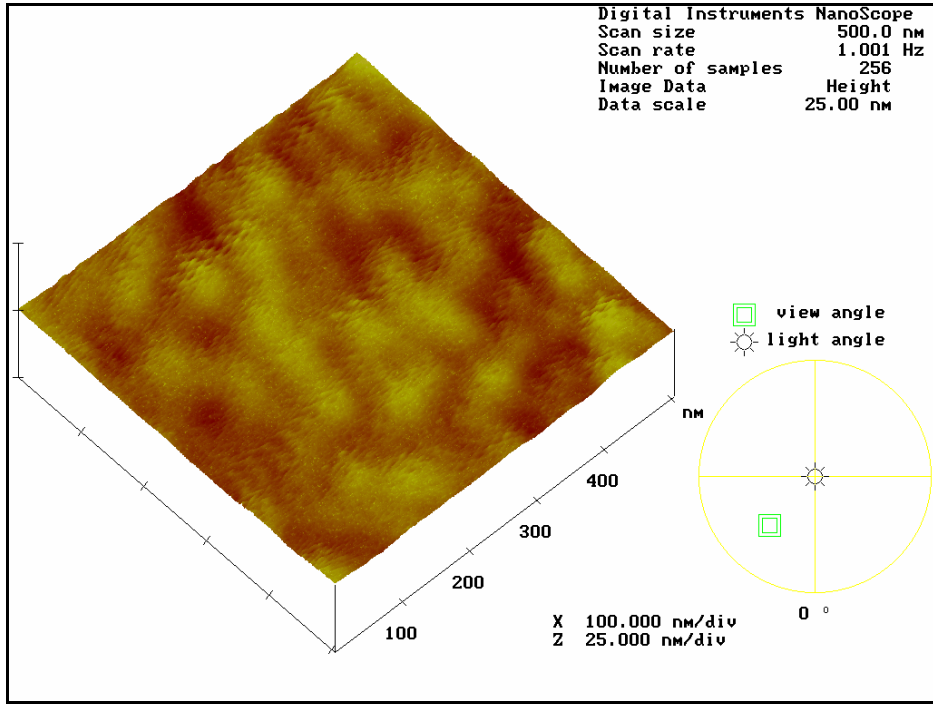


Figure 14: 3-D surface topography for W/NbN ($\Lambda=5.6$ nm) sample (pre-indentation).

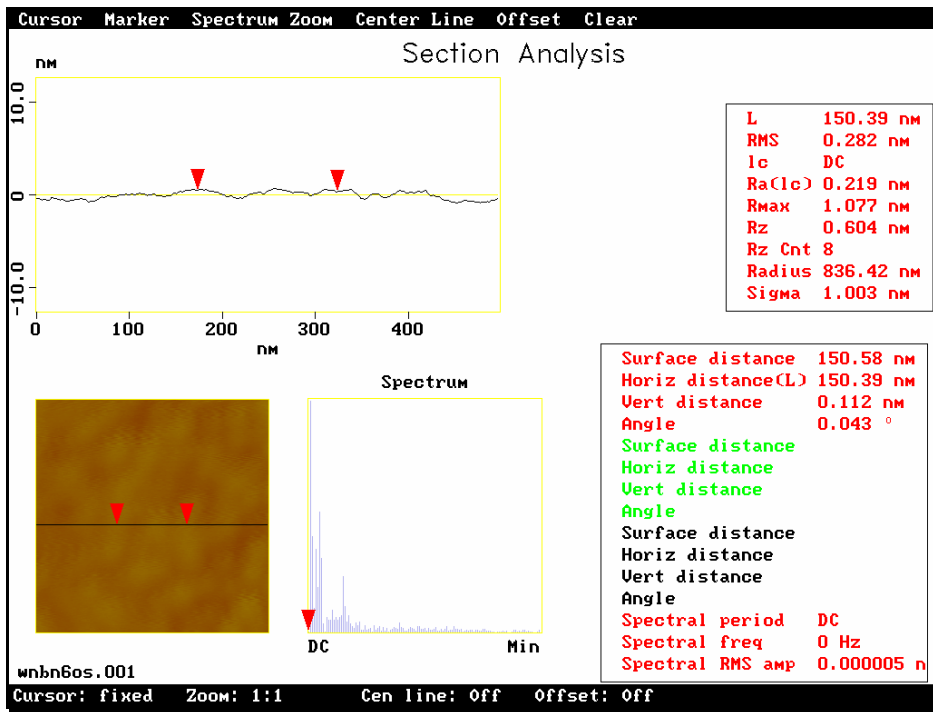


Figure 15: Typical section of surface for W/NbN ($\Lambda=5.6$ nm) sample (pre-indentation).

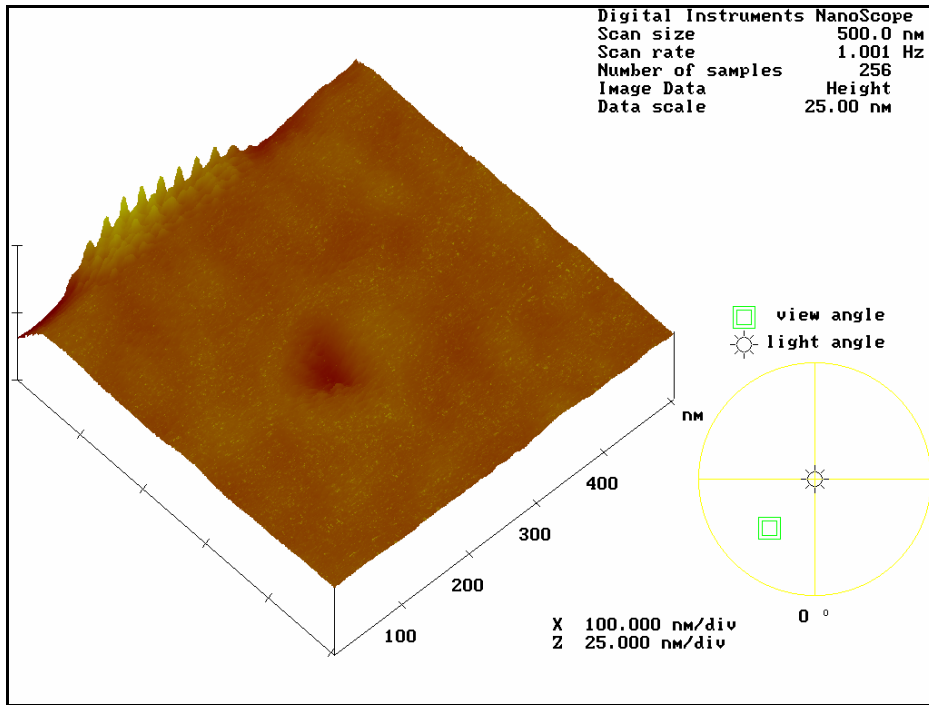


Figure 16: 3-D surface topography for W/NbN ($\Lambda=5.6$ nm) sample (post-indentation).

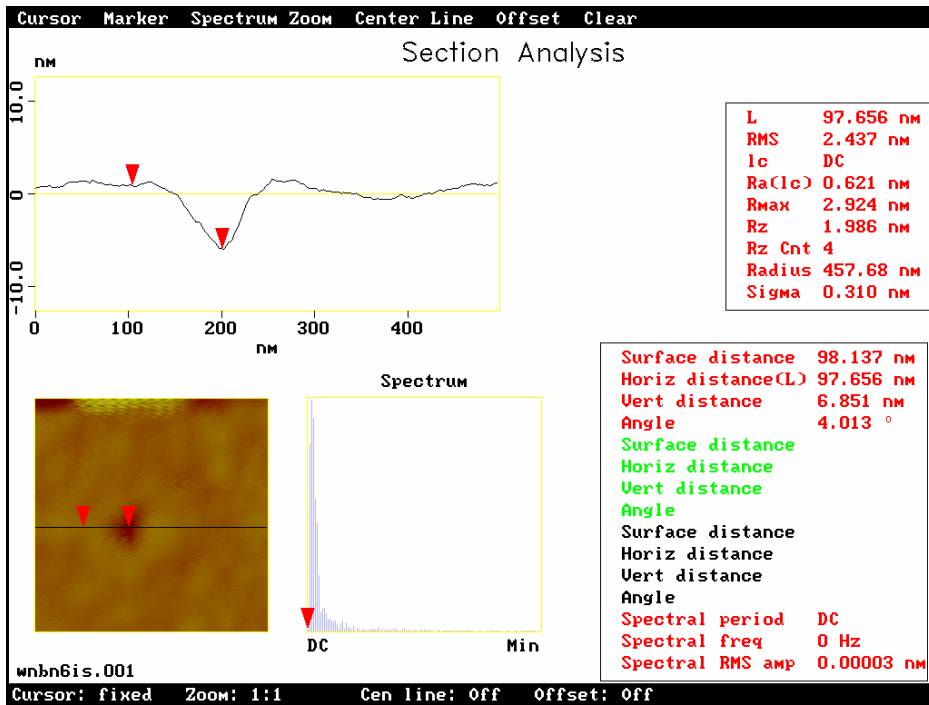


Figure 17: Typical section of surface for W/NbN ($\Lambda=5.6$ nm) sample (post-indentation).

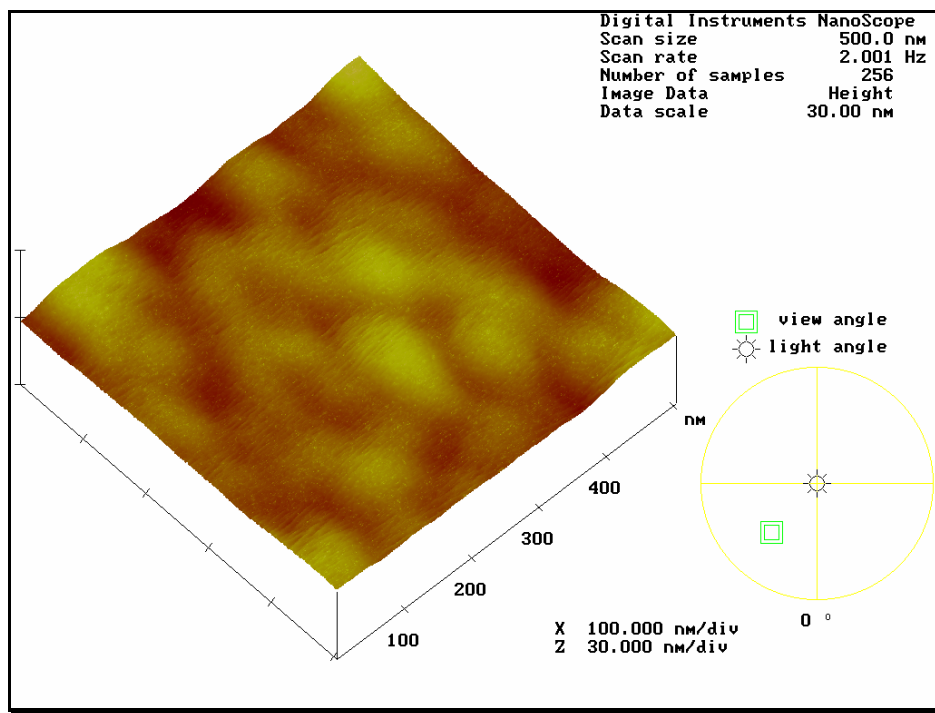


Figure 18: 3-D surface topography for W/NbN ($\Lambda=10.4$ nm) sample (pre-indentation).

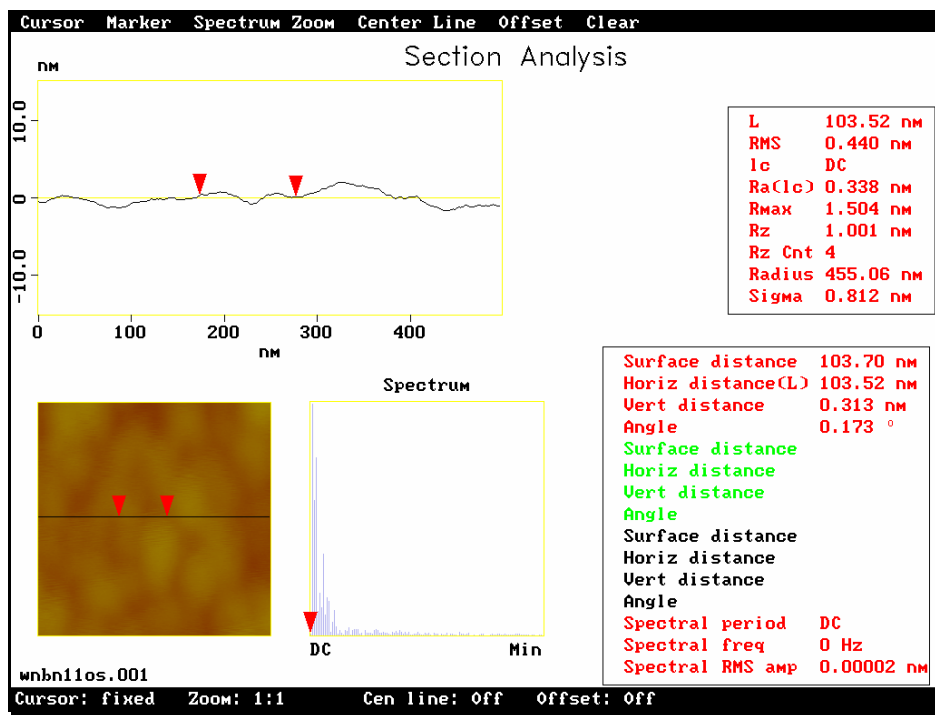


Figure 19: Typical section of surface for W/NbN ($\Lambda=10.4$ nm) sample (pre-indentation).

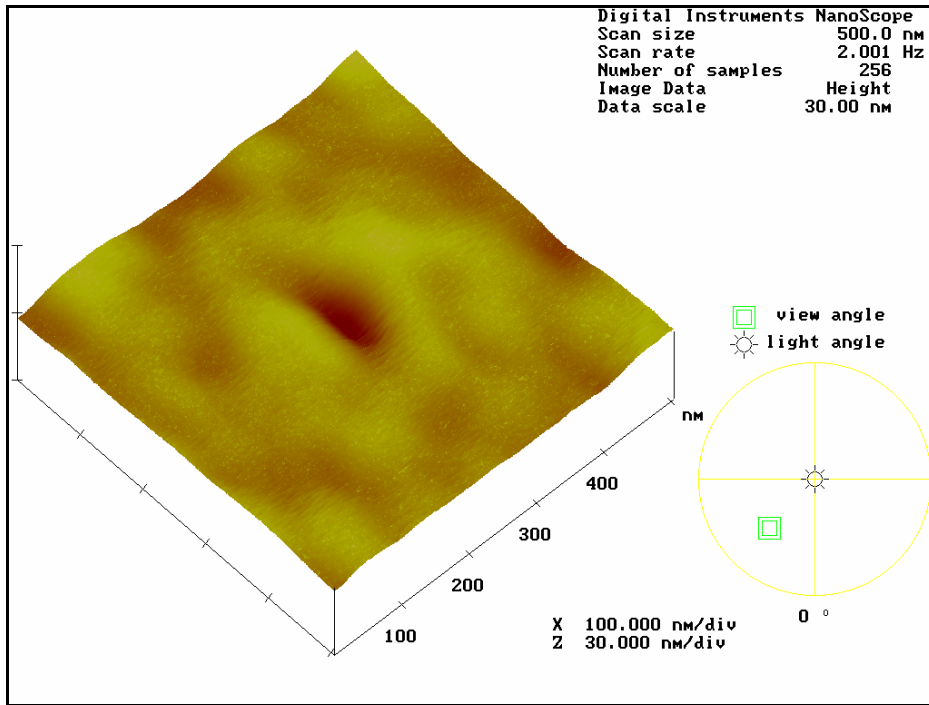


Figure 20: 3-D surface topography for W/NbN ($\Lambda=10.4$ nm) sample (post-indentation).

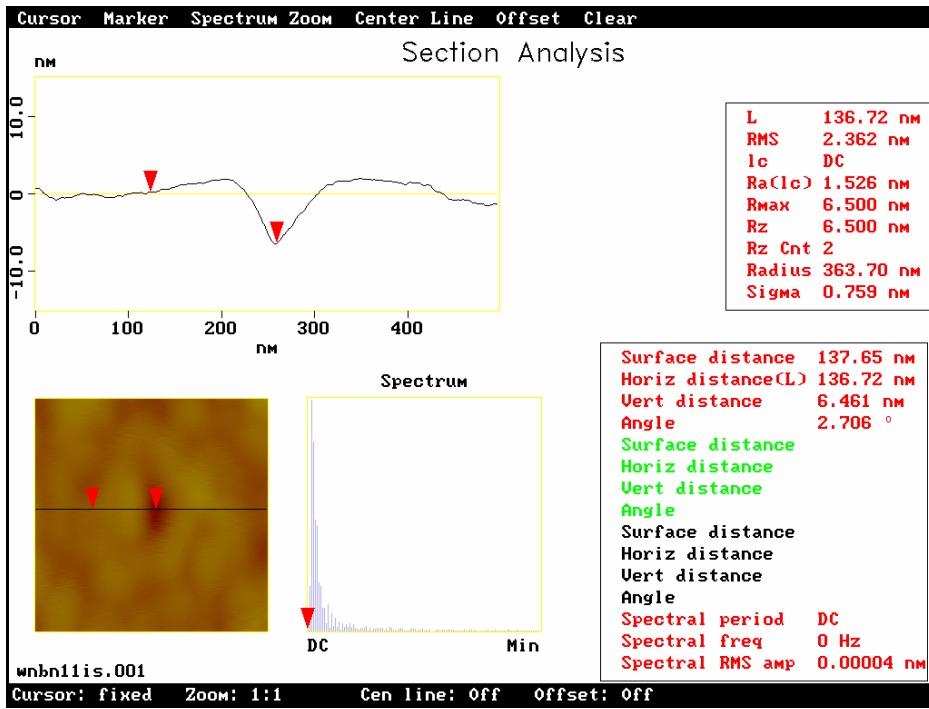


Figure 21: Typical section of surface for W/NbN ($\Lambda=10.4$ nm) sample (post-indentation).

4.0 EXPERIMENTAL RESULTS

The experimental data was obtained from two primary sources: the load versus displacement curves and the scanned surface images recorded after nanoindentation. The results of the experiments are presented in several parts. In the first section, the hardness of the different material samples is compared. In the second section, the reduced elastic moduli are compared. In the third section, the load versus displacement curves are examined in several ways using different combinations. In the fourth section, the energy of indentation is calculated from the load versus displacement curves and the results compared for all the materials. In the last section, the material pile-up around the indentation areas is examined.

In the Figures comparing the experimental results, the properties of the samples are generally presented as a function of either the *final* or *maximum* indentation depth. This information is obtained from the load versus displacement curves. These terms are defined in Figure 4 using a typical load versus displacement curve. The maximum indentation depth, h_{\max} , is the maximum penetration of the indenter tip into the material sample achieved during nanoindentation. The final indentation depth, h_f , is defined as the permanent deformation remaining after the applied load is removed and any elastic recovery of the material has occurred.

4.1 Hardness

Hardness is a general measure of the resistance of a material to plastic deformation. As noted earlier, the hardness is normally defined as the ratio of the maximum applied load divided by the corresponding projected contact area. The hardness was calculated from the unloading portion of the load versus displacement curve using a calibrated area function. A comparison of the hardness as a function of the maximum indentation depth is shown in Figure 22 for the indentations from Stage 1 of the experiment.

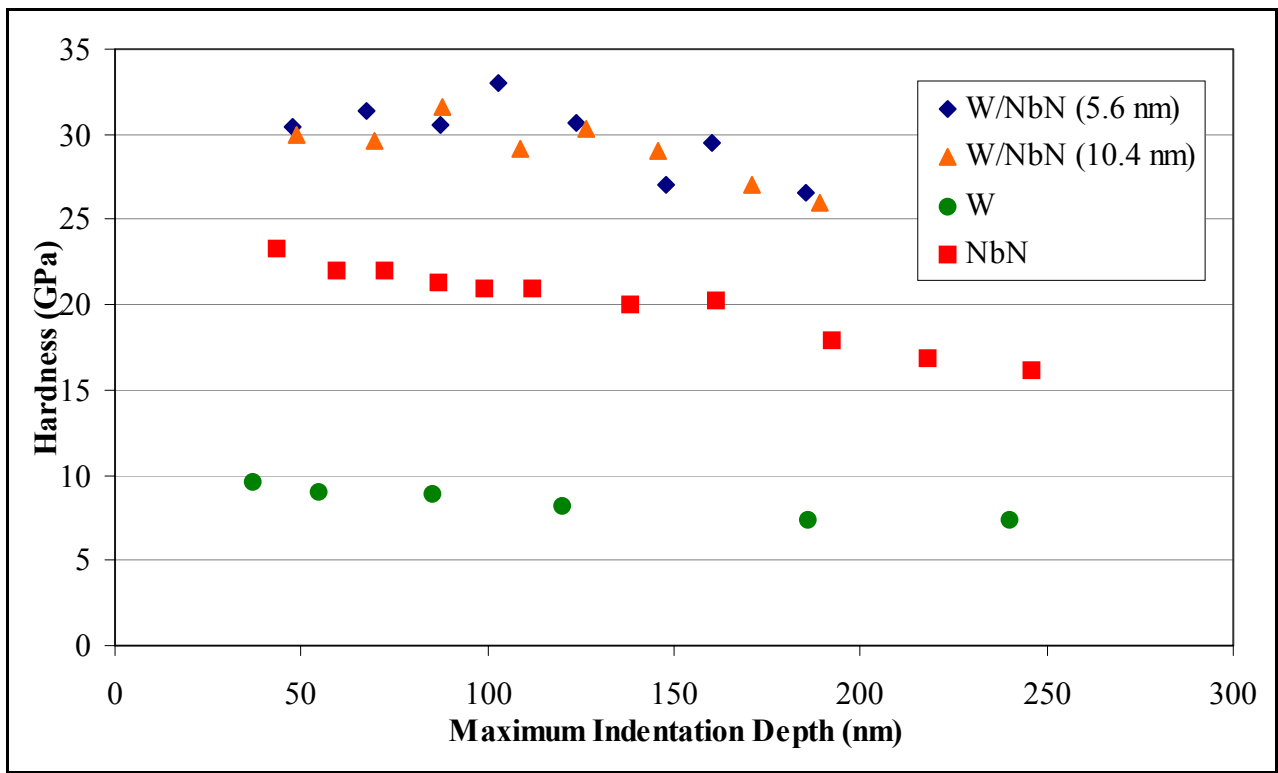


Figure 22: Hardness as a function of maximum indentation depth (Stage 1 indentations).

An examination of this graph shows several trends. The results for the monolithic material samples, NbN and W, indicate the presence of the Indentation Size Effect (i.e. there is increase in hardness as the indentation depth decreases). The tungsten hardness ranges from approximately 7 GPa at an indentation depth of 240 nm and gradually increases to about 10 GPa at a depth of 40 nm. The niobium nitride hardness ranges from 17 GPa at a penetration depth of 250 nm to about 23 GPa at a depth of 40 nm. In contrast, the behavior of the nanocomposites differs from the behavior for the monolithic materials. The hardness for both nanocomposites is consistent over a range of indentation depth (50 nm to approximately 150 nm) before it begins to taper off slightly. The final observation is that the hardness for each sample at the deeper indentation depths approaches the microhardness reported in the literature (See Table 1 above).

A comparison of the hardness as a function of the maximum indentation depth for all the material samples for the shallow nanoindentations (Stage 2) is shown in Figure 23. Again, the hardness for each indentation was calculated using a calibrated area function. A comparison of the results shows no significant difference in the hardness for the two superlattice samples (W/NbN, $\Lambda=5.6$ nm and W/NbN, $\Lambda=10.4$ nm) and the NbN sample for the shallow indentation depths (less than 25 nm). Also, the Indentation Size Effect causes the hardness of W to increase until it is approximately the same as the hardness of NbN (at 5 nm).

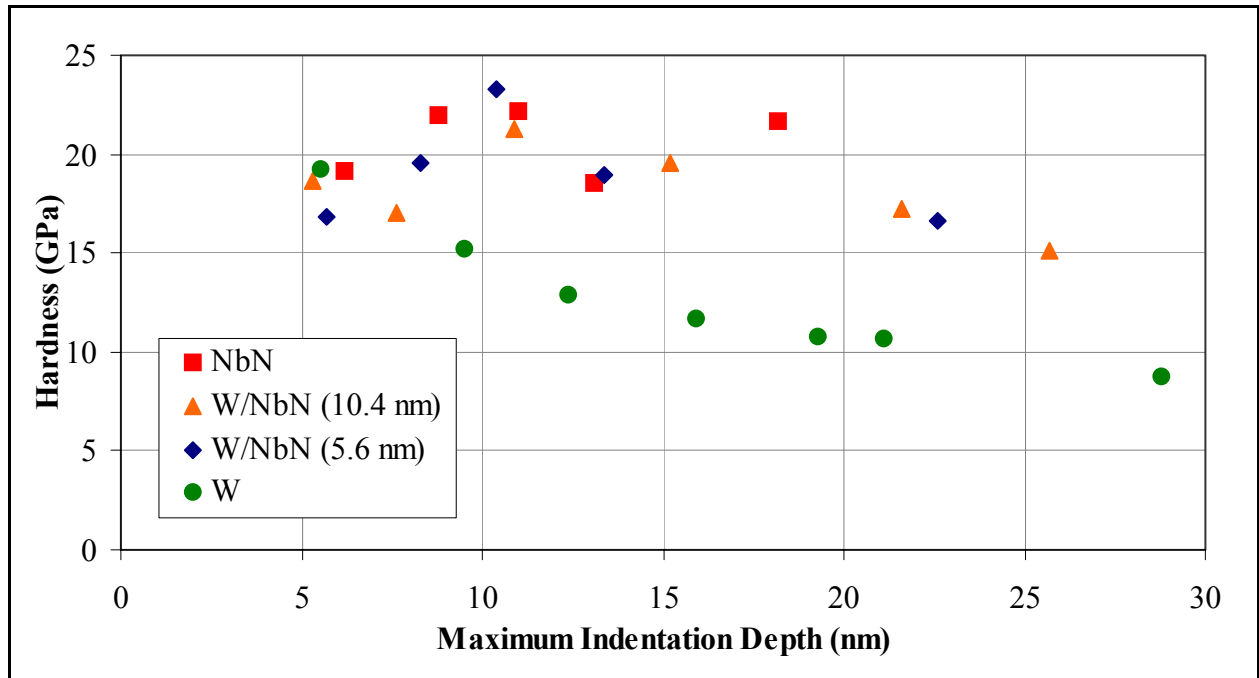


Figure 23: Hardness as a function of maximum indentation depth (Stage 2 indentations).

Combining the results of the previous two graphs (Figures 22 & 23), some deductions can be made regarding the factors contributing to the observed hardness increase in the superlattice materials. Both W and NbN exhibit hardness around 20-23 GPa at an indentation depth of 5 nm. This is the approximate thickness of an individual layer in one of the superlattice materials and both superlattice materials exhibit similar hardness at the same indentation depths. The influence of the interfaces is minimal for the shallow indentations because only a few interfaces are in the load zone and the amount of plasticity is small. However, at the deeper indentation depths, the hardness increases for the superlattice materials. Since the number of interfaces in the load zone increases at deeper indentation depths, this indicates that the interface between layers is an important factor in the remaining increase in hardness observed in the superlattice materials. The results suggest that there is some transition point between 25 nm and

50 nm where the interface begins to enhance the resistance to deformation, thereby causing the increase in hardness. Further experimentation would be required to confirm this hypothesis.

4.2 Elastic Moduli

The other mechanical property that can be determined from the unloading portion of the load versus displacement curve using the Oliver and Pharr method [17] is the reduced elastic modulus. In general, the elastic moduli should be constant regardless of the indentation depth, although some minor variation is to be expected due to material imperfections. The reduced elastic moduli for the indentations from Stages 1 and 2 were calculated using the calibrated area functions and compared for all the samples (shown in Figure 24).

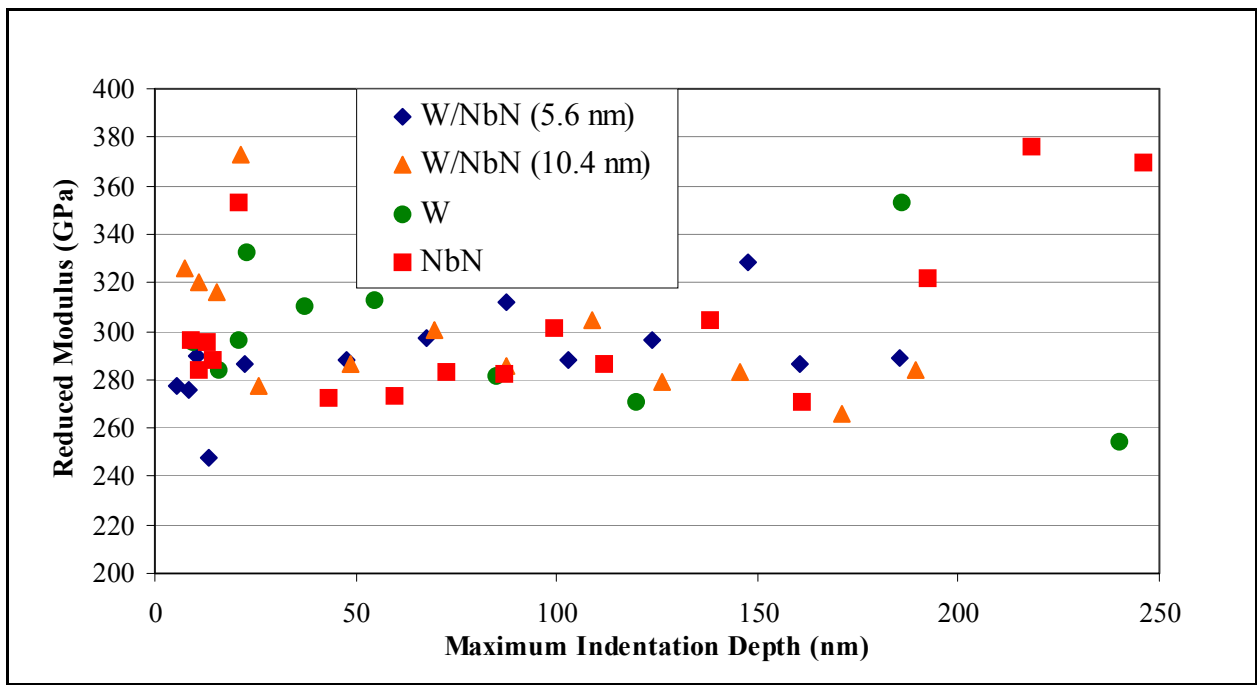


Figure 24: Comparison of the reduced modulus for each sample.

Since some of the data in Figure 24 is scattered, the means and standard deviations for the elastic moduli were calculated for each sample. The results are presented in Table 6.

Table 6: Summary statistics for Reduced Moduli.

	W	NbN	W/NbN ($\Lambda=5.6$ nm)	W/NbN ($\Lambda=10.4$ nm)
Reduced Modulus, Mean	309.0 GPa	299.4 GPa	289.3 GPa	310.3 GPa
Reduced Modulus, Std. Dev.	50.55 GPa	29.98 GPa	18.81 GPa	46.99 GPa

Since the properties of the indenters are known (i.e. Young's Modulus is 1140 GPa and Poisson's ratio is 0.07 for diamond), the theoretical value of the reduced modulus can be computed from the equation (4). Using equation (2) and the values from Table 2, the calculated reduced modulus for W is 309 GPa. This agrees with the mean value of the elastic modulus for W determined from the experimental data in Table 6. An examination of the data in Figure 24 and Table 6 shows that the majority of the data falls between 270 GPa and 310 GPa. These results indicate that there is some difference in the elastic moduli for the materials. However, the difference in elastic moduli is not very large. Therefore, while the elastic modulus may still have a small influence on the hardness, it should not be considered as the dominant factor in explaining the entire increase in hardness observed in the nanocomposites.

4.3 Load vs. Displacement Curves

In the preceding section, the unloading portion of the load versus displacement curves was used to determine two mechanical properties: the hardness and the elastic moduli. However, in this case, several additional observations concerning the behavior of the superlattice materials can be made from the load versus displacement curves. This was done by examining different combinations of the curves of the two nanocomposites and their monolithic components. The load versus displacement curves for the shallow indentations (Stage 2) will be considered first. Comparisons of the load versus displacement curves for NbN and W at shallow indentation depths with each nanocomposite, W/NbN ($\Lambda=5.6$ nm) and W/NbN ($\Lambda=10.4$ nm), are shown in Figure 25 and Figure 26 respectively.

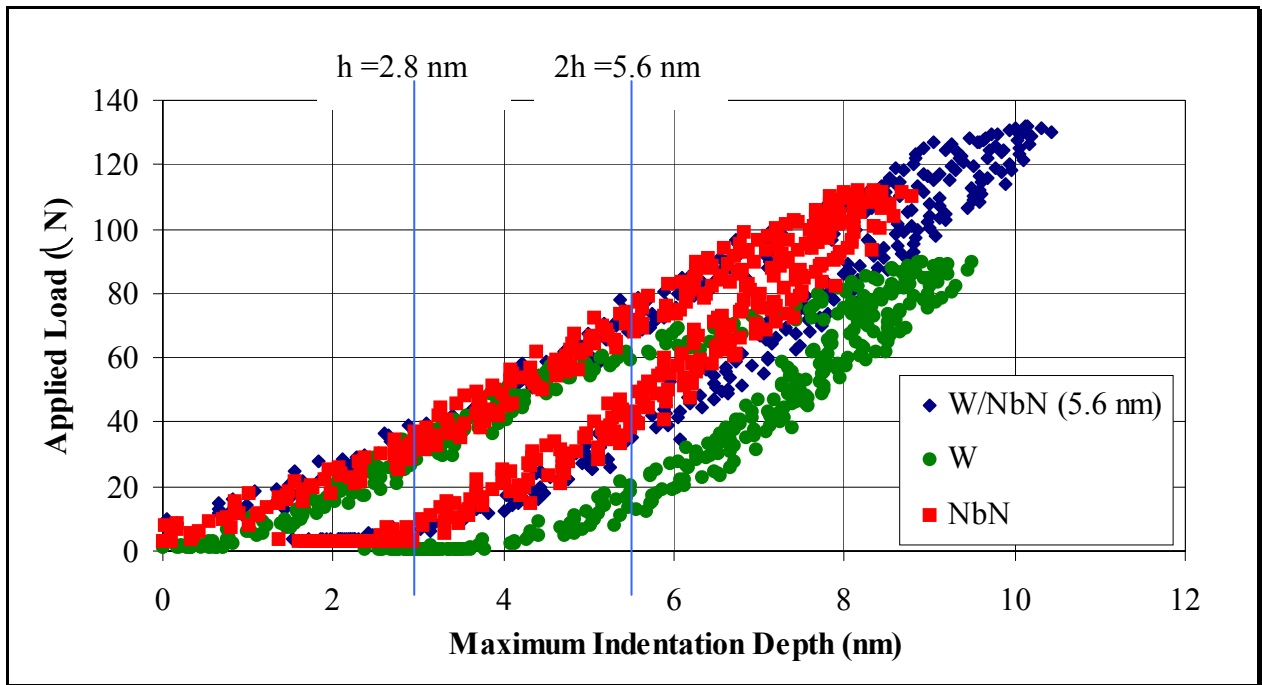


Figure 25: Comparison of load vs. displacement data for W/NbN ($\Lambda=5.6$ nm) sample.

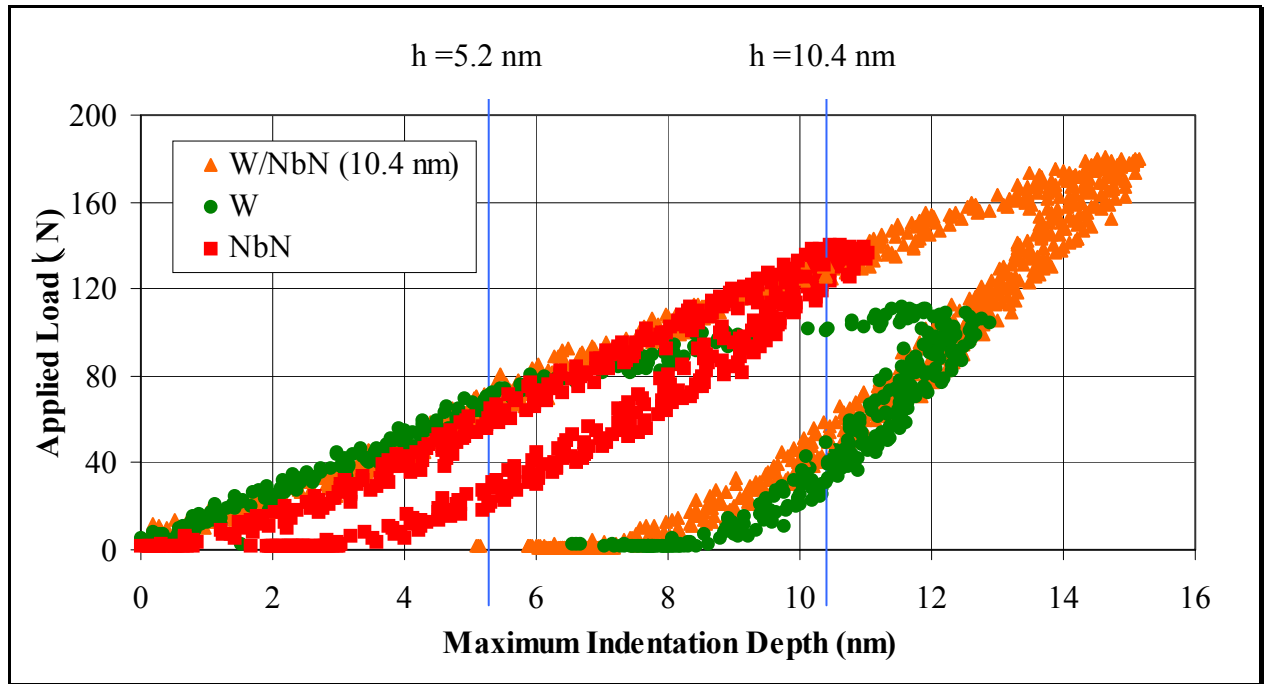


Figure 26: Comparison of load vs. displacement data for W/NbN ($\Lambda=10.4$ nm) sample.

In both cases, the comparison of the load versus displacement curves indicate that the superlattice materials, W/NbN ($\Lambda=5.6$ nm) and W/NbN ($\Lambda=10.4$ nm), exhibit loading and unloading patterns which are very similar to the behavior of NbN. Both comparisons also demonstrate that tungsten initially follows the same loading pattern but starts to deviate from the others at approximately 5 nm. Since the bilayer repeat periods for W/NbN ($\Lambda=5.6$ nm) and for W/NbN ($\Lambda=10.4$ nm) are so shallow, the indenter has penetrated only a couple of layers into the superlattice materials.

Proceeding to the deeper indentations made in Stage 1, a comparison of the load versus displacement curves for all the samples at two different indentation depths is shown in Figure 27.

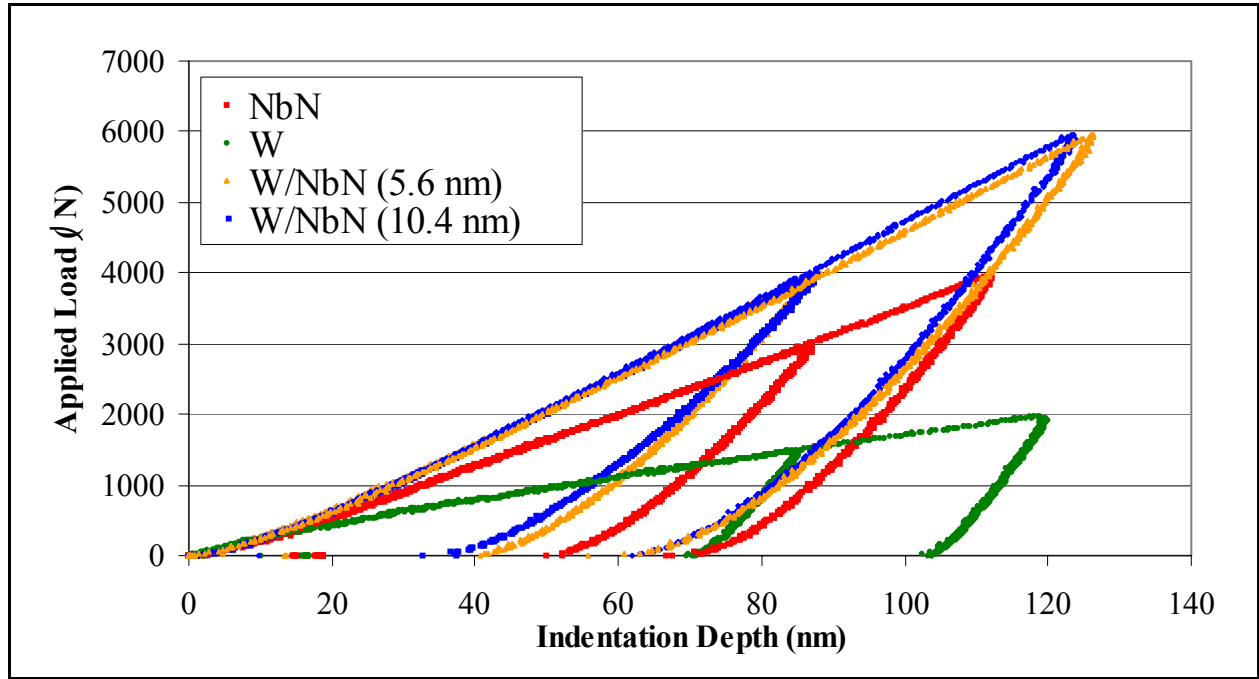


Figure 27: Comparison of load vs. displacement data for same indentation depth.

Examining this graph, there appears to be little difference in the initial section of the loading portion of the curves. This agrees with the data from the shallow indentations. At an indentation depth of about 20 nm, the loading portions of the curves begin to diverge. The data also shows that the nanocomposites require a greater load to achieve the same maximum penetration of the indenter into the samples. Furthermore, a comparison of the indentations for the same applied load shows that there is very little difference in the maximum indentation depth for the superlattice samples W/NbN ($\Lambda=5.6$ nm) and W/NbN ($\Lambda=10.4$ nm) for a specific load.

A comparison of the load versus displacement curves for all the samples for the same applied load is shown in Figure 28. As expected, the nanocomposites permit the least amount of indenter penetration, while the tungsten permits the most. Also, it is evident that there is little difference in penetration depth for the nanocomposites.

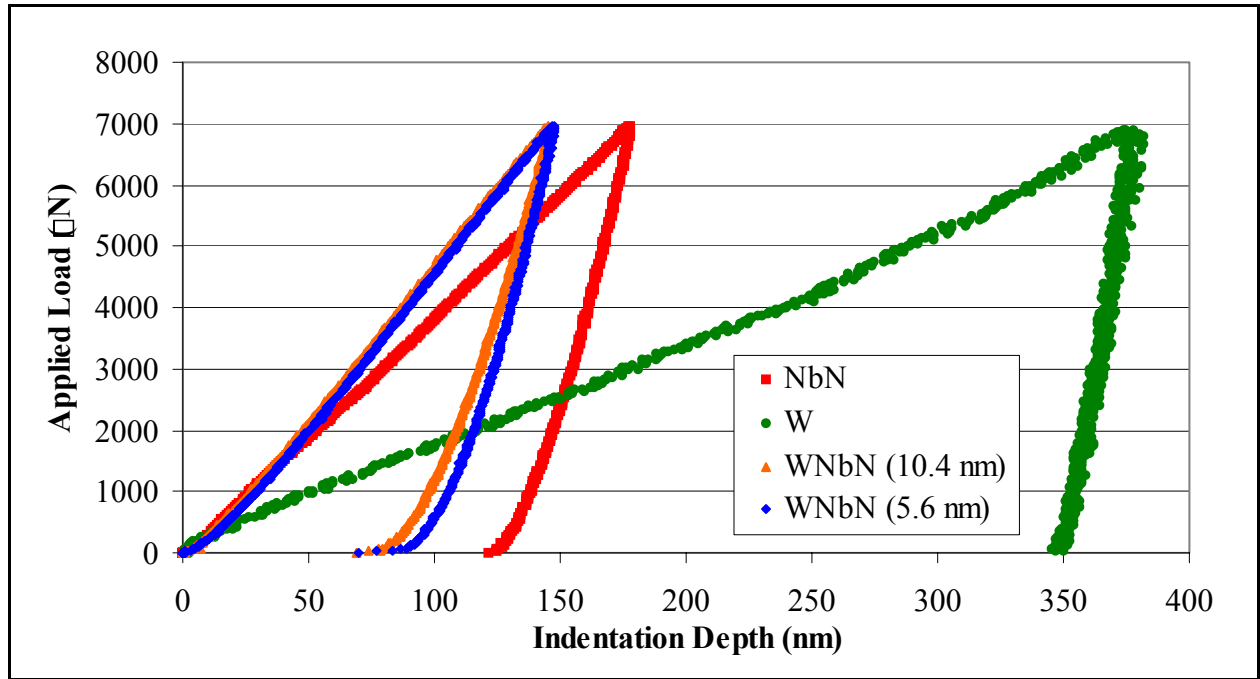


Figure 28: Comparison of load vs. displacement data for same load.

Another useful comparison is the load versus displacement curves for all the samples based on the same *final* indentation depth (i.e. same permanent deformation). This was done for all the samples at four different final indentation depths: 3 nm, 8 nm, 13 nm and 110 nm. These comparisons are shown in Figures 29, 30, 31 and 32 respectively.

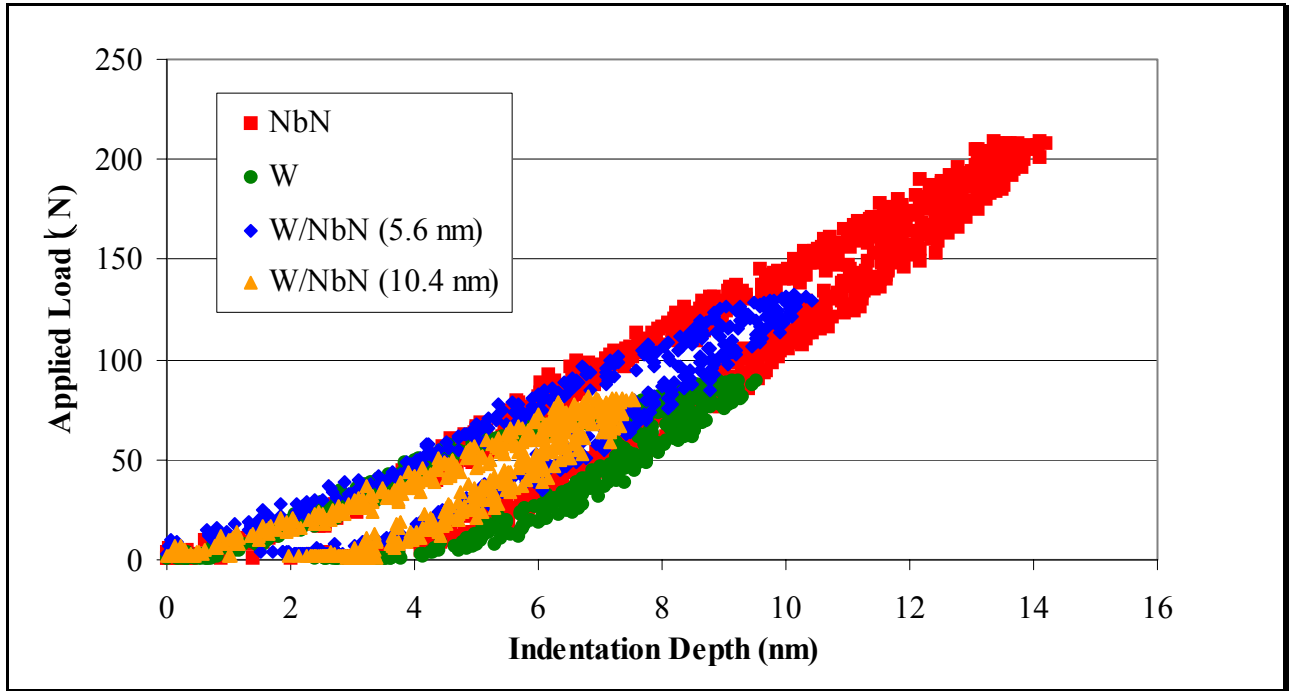


Figure 29: Comparison of load vs. displacement data for final indentation depth of 3 nm.

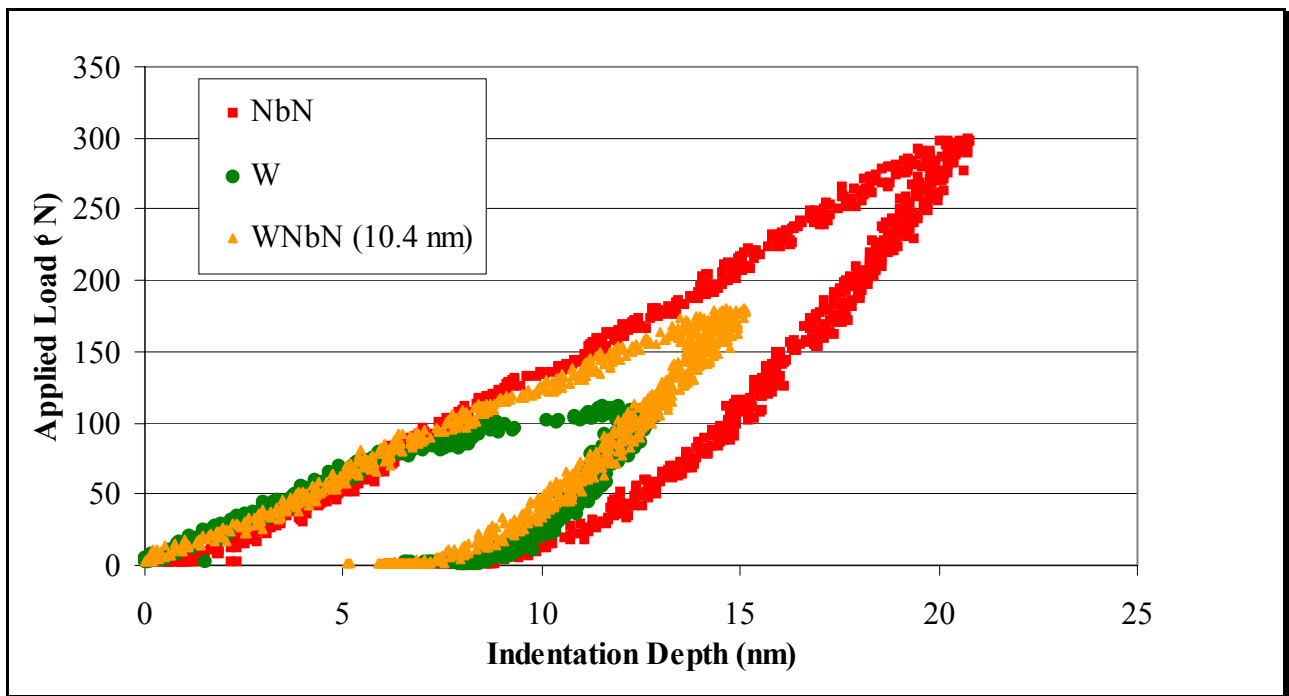


Figure 30: Comparison of load vs. displacement data for final indentation depth of 8 nm.

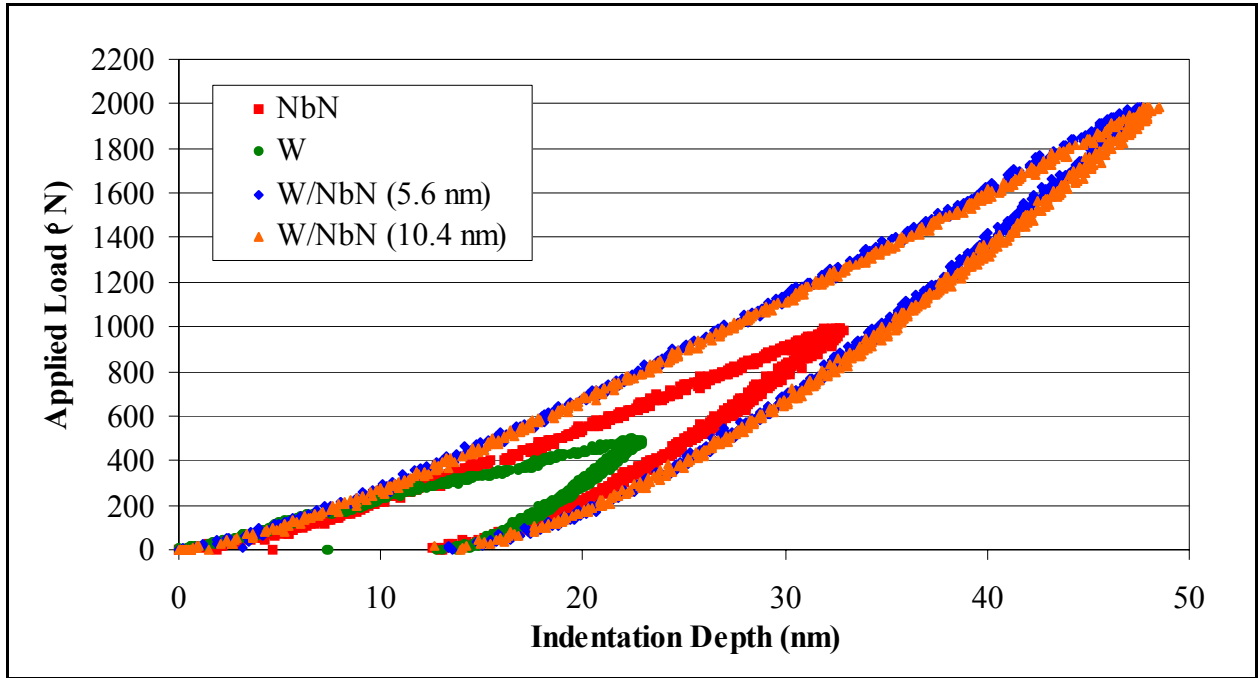


Figure 31: Comparison of load vs. displacement data for final indentation depth of 13 nm.

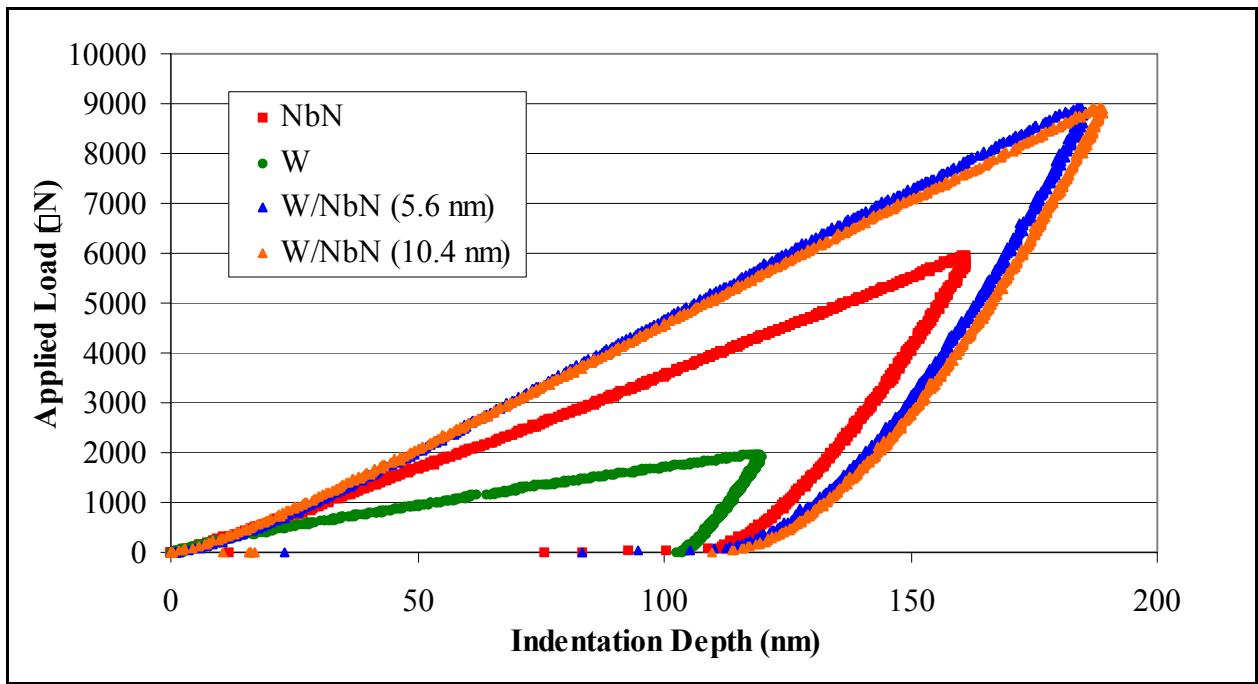


Figure 32: Comparison of load vs. displacement data for final indentation depth of 110 nm.

An examination of these four comparisons of the load versus displacement curves shows an interesting phenomenon. For the shallow indentations (Figures 29 and 30), the NbN actually requires the deepest penetration of the indenter to achieve the same *final* indentation depth (or the same permanent deformation). However, as the indentation depth increases (Figures 31 and 32), the two superlattice materials, W/NbN ($\Lambda=5.6$ nm) and W/NbN ($\Lambda=10.4$ nm), require the deepest penetration. This may be the result of the number of the interfaces in the load zone. At shallow indentation depths, few interfaces are in the deformation zone and the dislocation movement required to accommodate the plastic deformation is minimal. However, as the penetration depth increases, the amount of dislocation activity increases. At some point, the behavior of the interface as a barrier to dislocation motion begins to affect the deformation characteristics of the nanocomposites leading to the observed increase in hardness. These comparisons also imply that it may be beneficial to consider the behavior of the materials in terms of the energy required to generate the plastic deformation. This issue will be discussed in the next section.

Another indication of the relative amount of the elastic versus plastic deformation is the ratio of the *final* indentation depth, h_f , over the *maximum* indentation depth, h_{max} . A comparison was made of this ratio as a function of the maximum indentation depth for all the samples. As shown in Figure 33, the ratio is much lower for W/NbN ($\Lambda=5.6$ nm) and W/NbN ($\Lambda=10.4$ nm) than it is for NbN and W. This demonstrates that the presence of the interface affects the ratio of elastic/plastic behavior in the nanocomposites, and that the amount of elastic recovery is much greater for the superlattice materials than for the monolithic components.

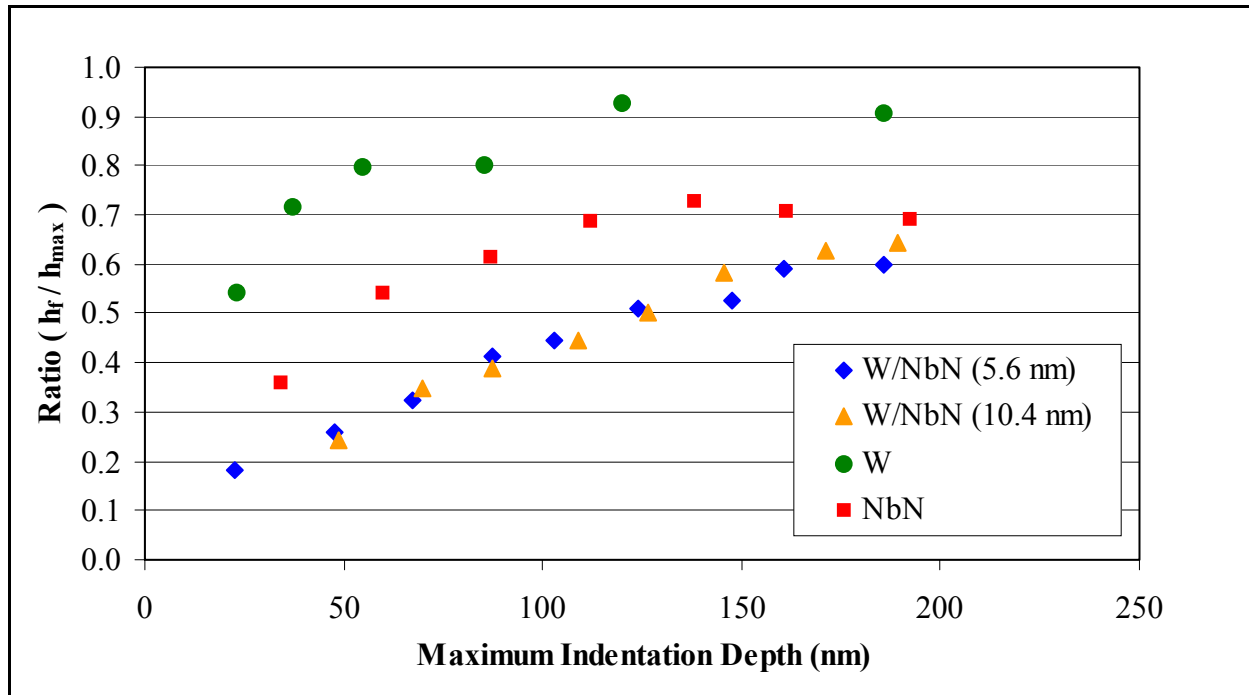


Figure 33: Ratio (h_f / h_{max}) as a function of maximum indentation depth.

4.4 Elastic / Plastic Energy of Indentation

As mentioned earlier, another method for evaluating the behavior of the nanocomposites is to consider the load versus displacement curves in terms of the elastic and plastic energy required to achieve a specific permanent deformation. Generally, the total energy of indentation is defined as the area under the loading portion of the curve; the plastic energy of indentation is defined as the area bounded by the loading and unloading portions of the curve; and the elastic energy is defined as the area under the unloading portion of the curve. [18] A typical load versus displacement curve for an indentation on a hard material is shown in Figure 34 with the areas used to determine the plastic and elastic areas labeled.

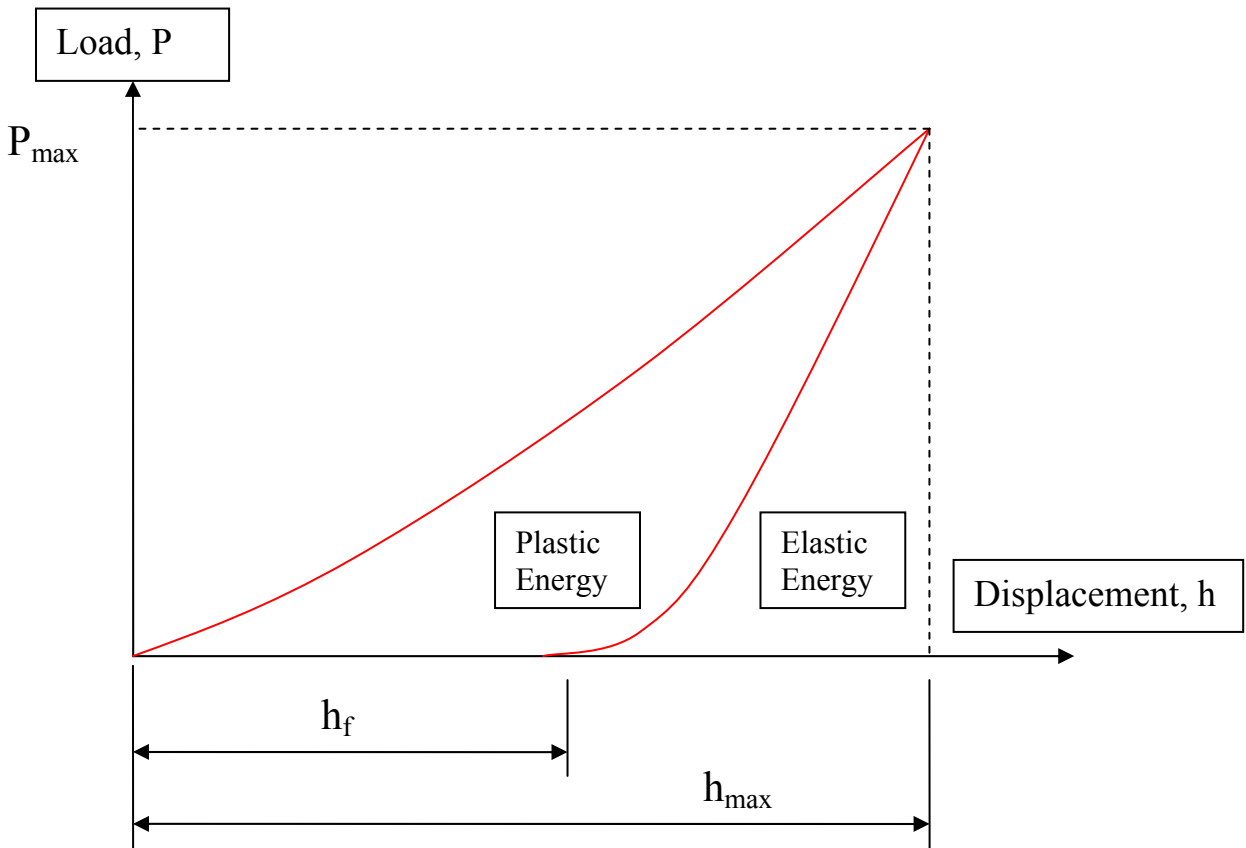


Figure 34: Definitions for energy of indentation.

As noted previously, the superlattice materials require a higher applied load to achieve the same final indentation depth as NbN or W at deeper indentations which is evident from the comparisons of the load versus displacement curves made in Figures 31 and 32. To pursue this topic further, the total, plastic and elastic energies were calculated for the Stage 2 indentations from the load versus displacement curve data. The areas under the curves were calculated from the indentation data using the Riemann's sum method using about a hundred data points to approximate the curve. A comparison of the total energy of indentation for the samples as a function of the final indentation depth is shown in Figure 35. The comparisons of the plastic and elastic energies of indentation are shown in Figure 36 and 37 respectively.

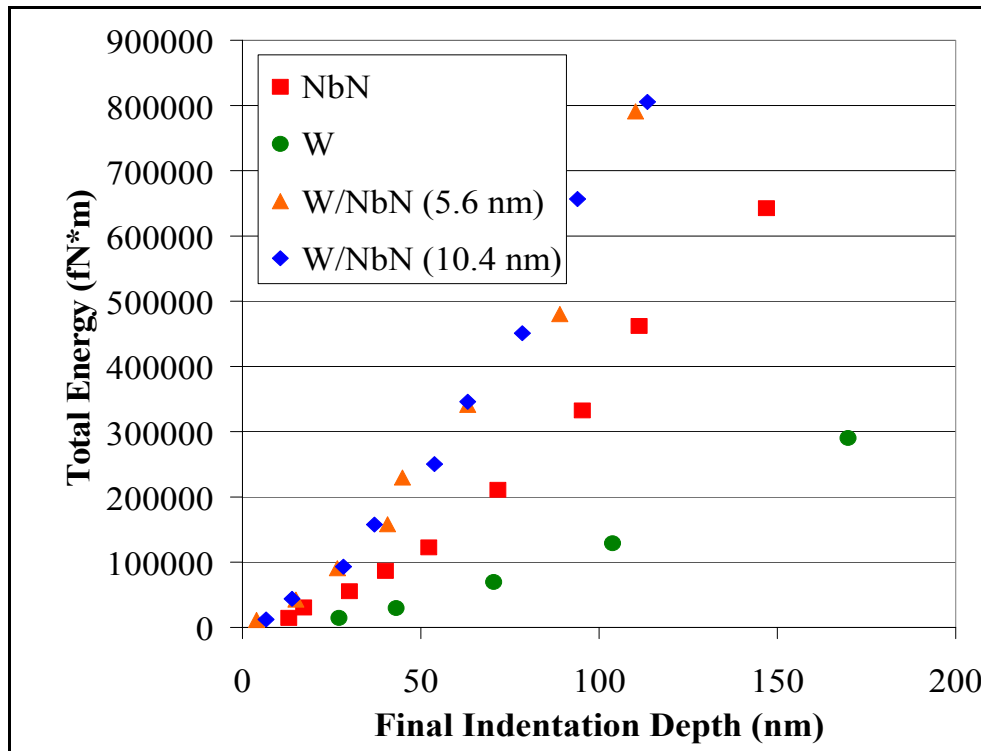


Figure 35: Comparison of the total energy of indentation as a function of h_f .

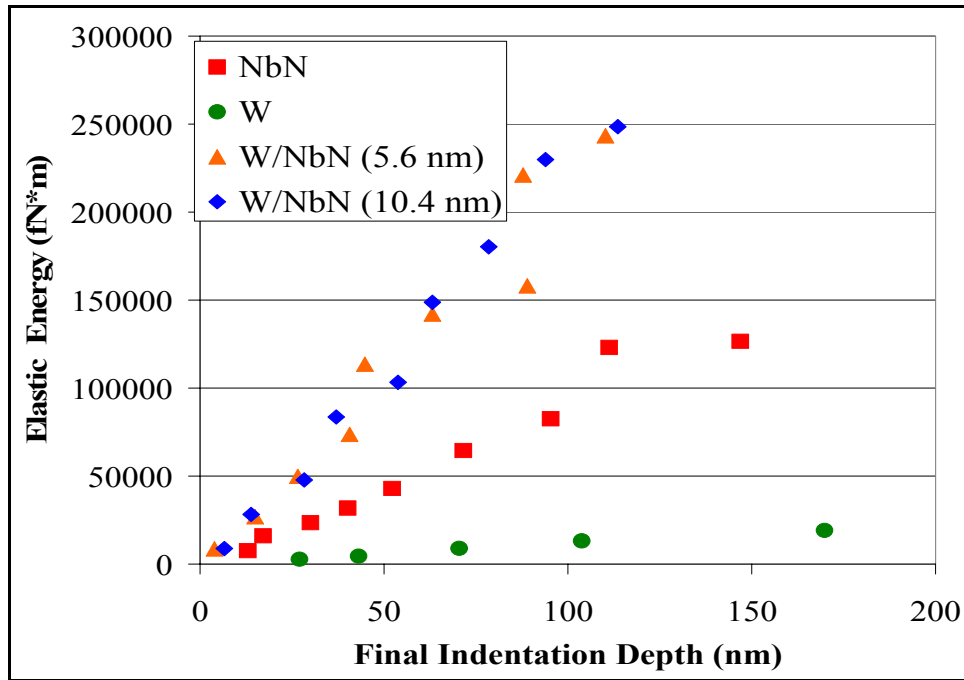


Figure 36: Comparison of the elastic energy of indentation as a function of h_f .

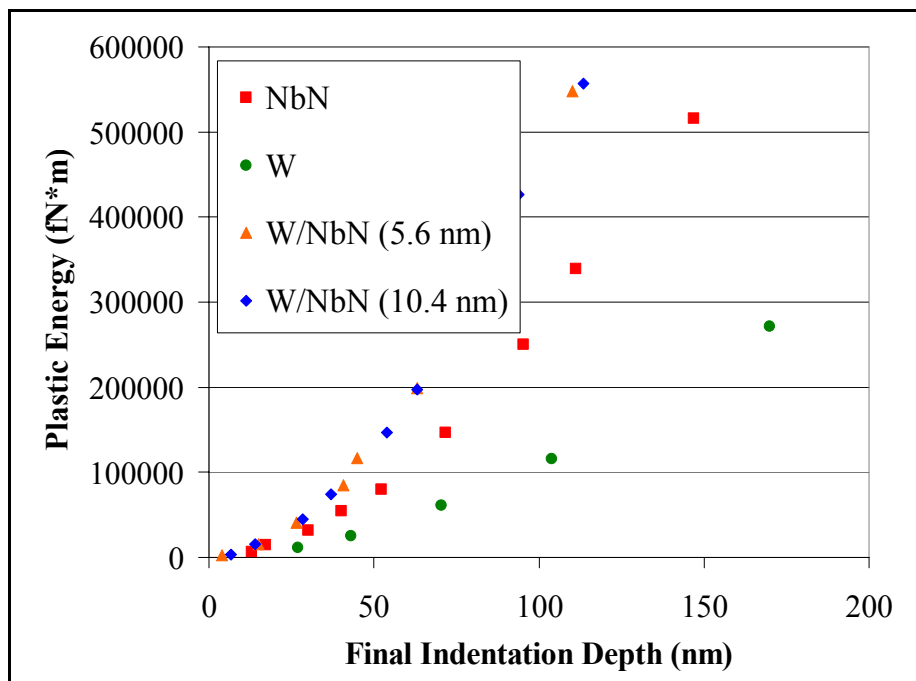


Figure 37: Comparison of the plastic energy of indentation as a function of h_f .

Several observations can be made from these comparisons. First, the total and plastic energies follow a power law pattern. This is consistent with the general observation in the literature that the applied load is proportional to the square of the indentation depth for a wide range of materials. Second, Figure 36 indicates that the elastic energy follows a linear pattern. Finally, although both the plastic and elastic energies are greater for the superlattice materials than for NbN, the elastic energy appears to have a greater relative influence on the superlattice materials. For example, at an indentation depth of 110 nm, the ratio of the plastic energy of indentation for the superlattice material to that of NbN is approximately 1.6 to 1. However, the ratio of the elastic energy of indentation for the superlattice material to that of NbN is approximately 2 to 1 for the same indentation depth. Consequently, the superlattice materials have a lower percentage of energy available for plastic deformation as shown in Figure 38.

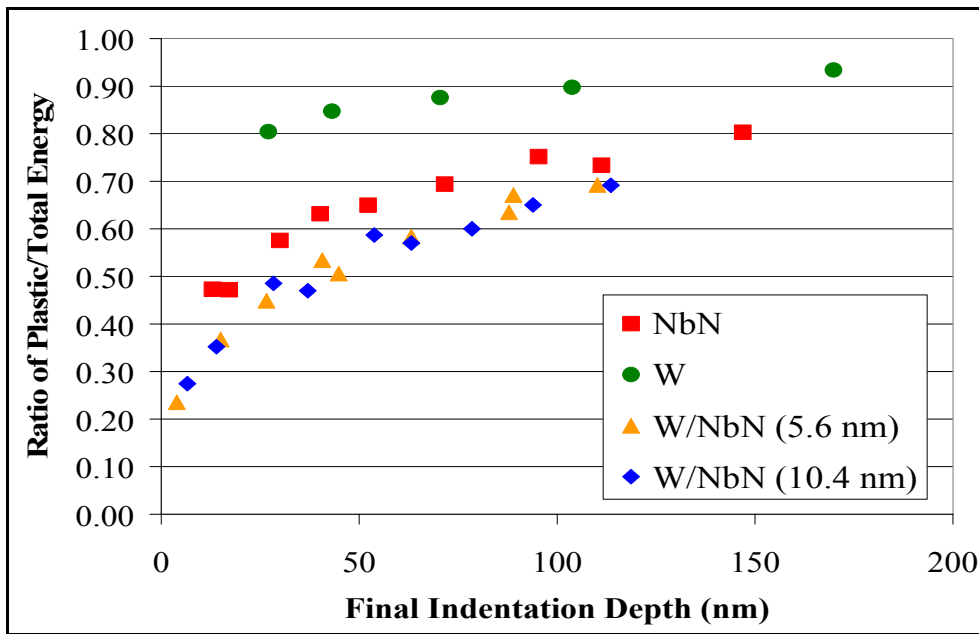


Figure 38: Comparison of the ratio of plastic energy/total energy as a function of h_f .

4.5 Material Pile-Up

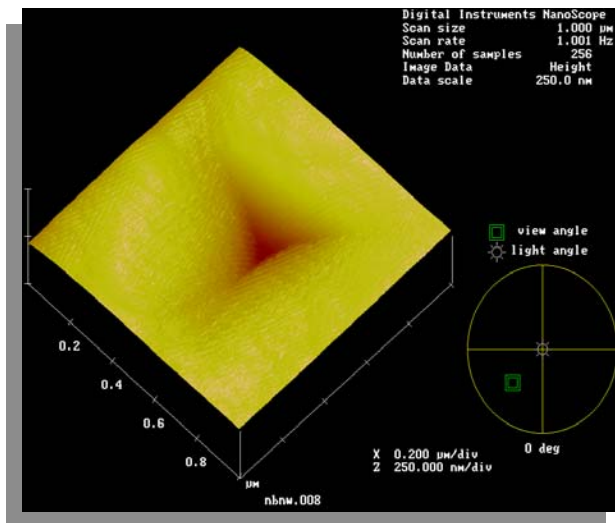
An examination of the scanned images shows significant pile-up of the material in the indentation area. The images shown in Figure 39 are for the same final indentation depth.



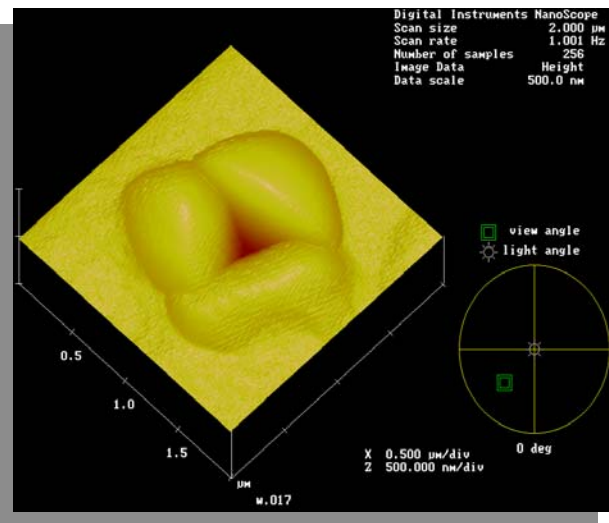
(a) W/NbN ($\Lambda=5.6$ nm) Sample



(b) W/NbN ($\Lambda=10.4$ nm) Sample



(c) NbN Sample



(d) W Sample

Figure 39: Comparison of pile-up for samples (a) thru (d) for same final indentation depth.

As can be seen from the scanned images in Figure 39, the NbN sample shows little evidence of material pile-up around the indentation area while the W/NbN ($\Lambda=5.6$ nm), W/NbN ($\Lambda=10.4$ nm) and W samples exhibit significant material pile-up. To examine this difference in deformation behavior, the pile-up height, t ; the radius at the maximum height of material pile-up, a ; and the approximate radius of the deformation zone, c were measured from the scanned images. A physical interpretation of these terms is shown in Figure 40. [19, 20]

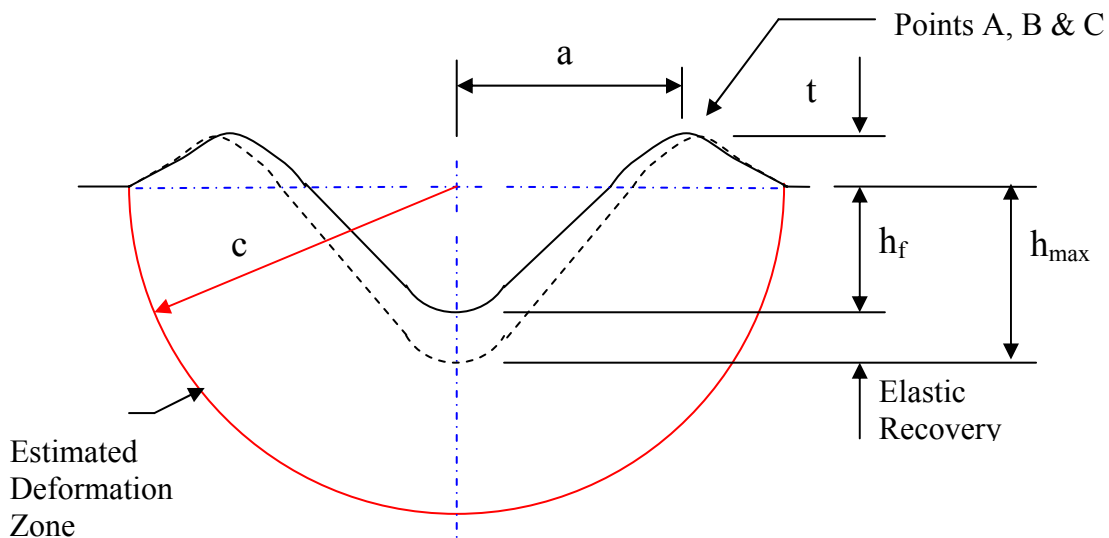


Figure 40: Definitions of pile-up terminology.

The section analysis tool of Digital Instruments was used to determine the values. For each indentation made in Stage 1 of the experiment, three cross sections were taken along a line bisecting the length of each leg of the triangle formed by the indenter and passing through the center of indentation. The orientations of these lines are shown in Figure 41. Points A, B and C

in Figures 40 and 41 indicate where the maximum pile-up was measured. Since the measured quantities were not the same for each cross section, average values were calculated for each term defined above.

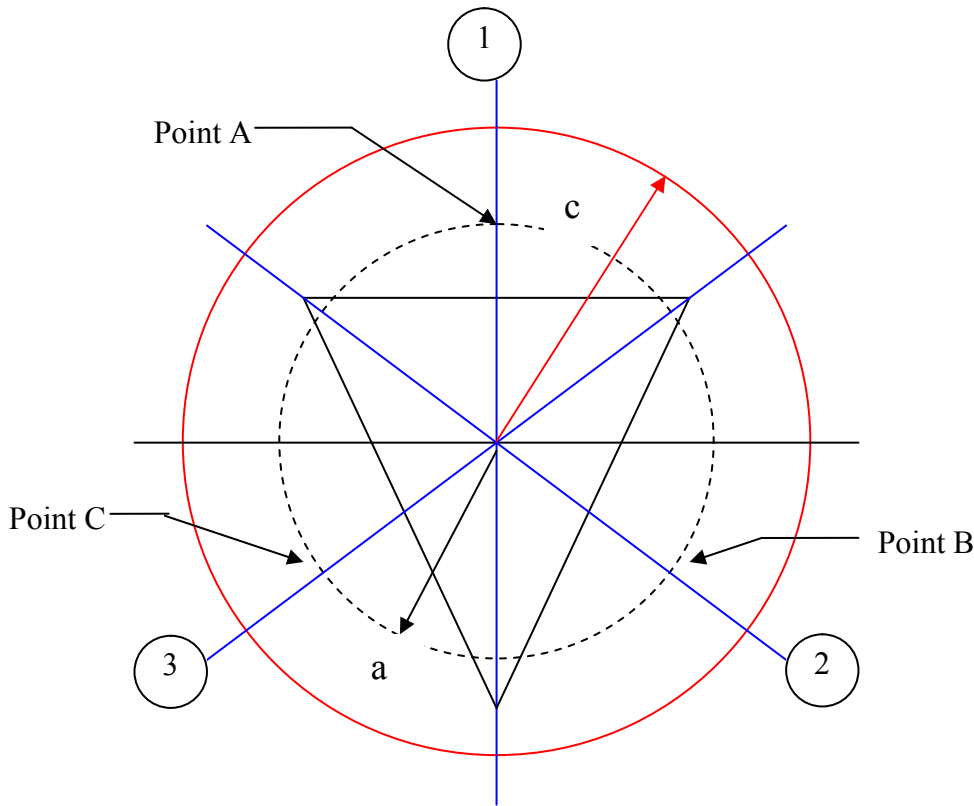


Figure 41: Sections used for pile-up analysis.

To evaluate the behavior of the material based on the pile-up, one graph was made for each geometric parameter to compare the material behavior of all the samples. The parameters examined are the pile-up height, t ; the ratio of the radius at the maximum pile-up height over the pile-up height, a/t ; and the ratio of the plastic zone radius over the pile-up height, c/t . These quantities were plotted both as a function of the *maximum* indentation depth (see Figures 42, 43 & 44), and as a function of the *final* indentation depth (see Figures 45, 46 & 47).

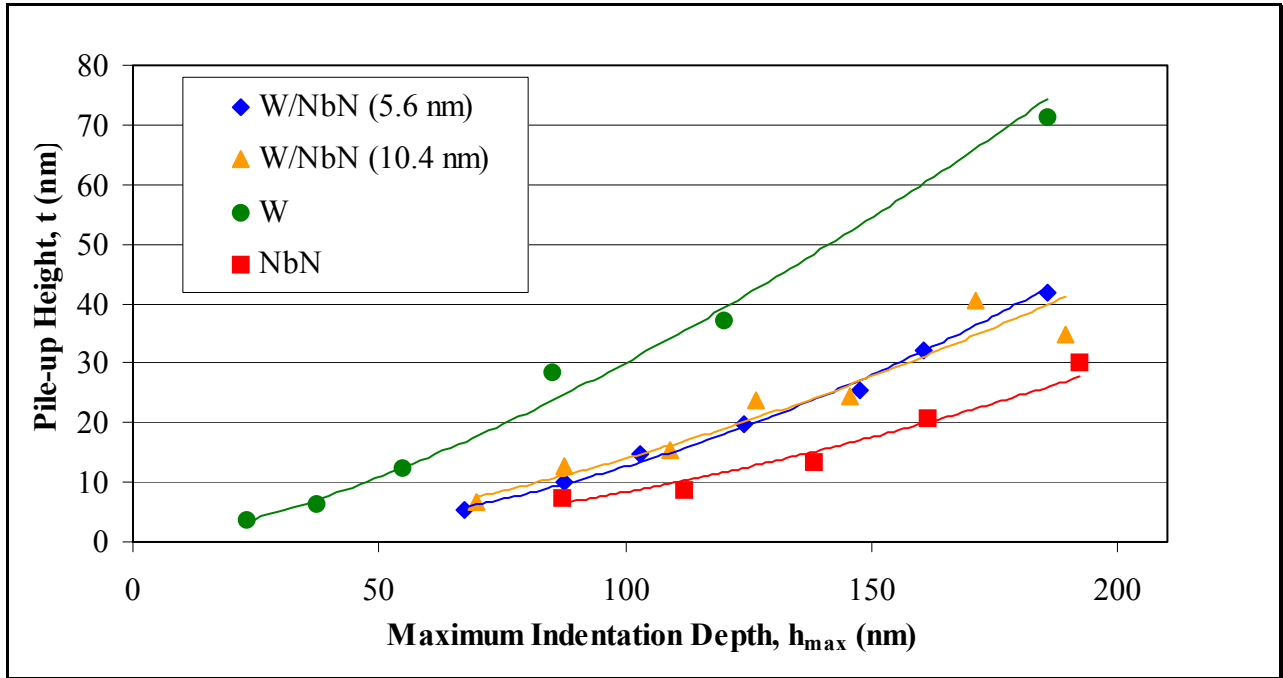


Figure 42: Pile-up Height, t , as a function of maximum indentation depth.

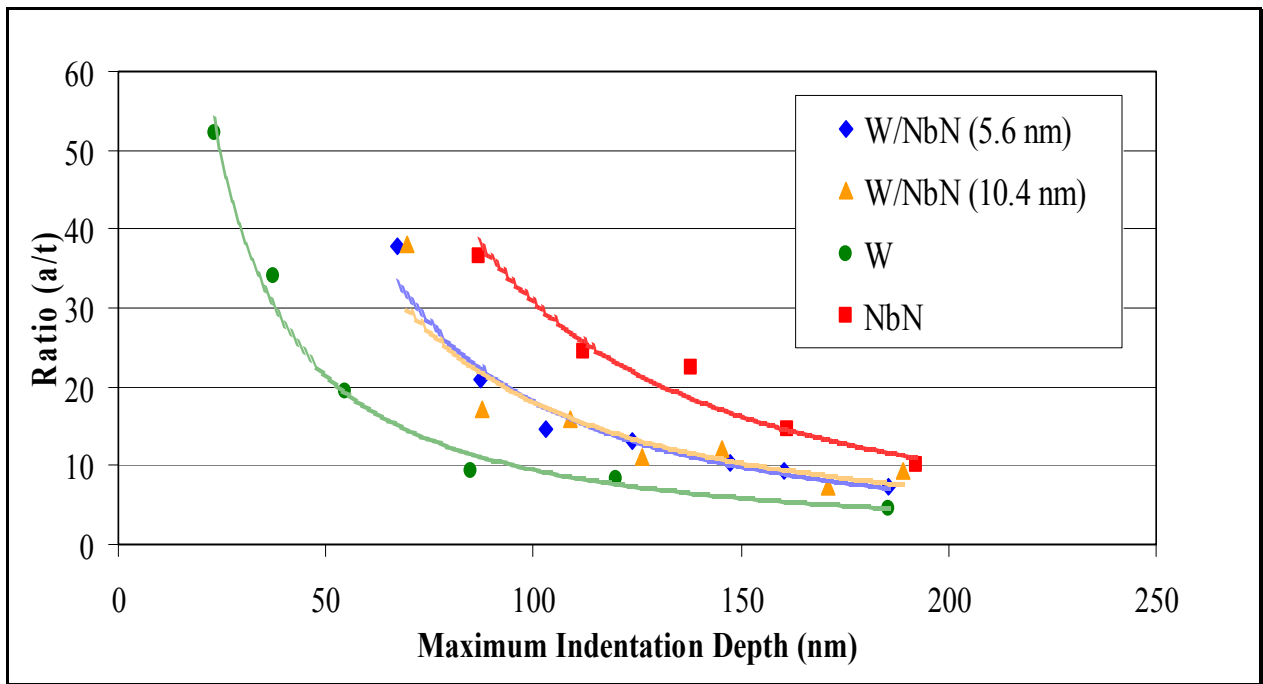


Figure 43: Ratio (a/t) as a function of maximum indentation depth, h_{max} .

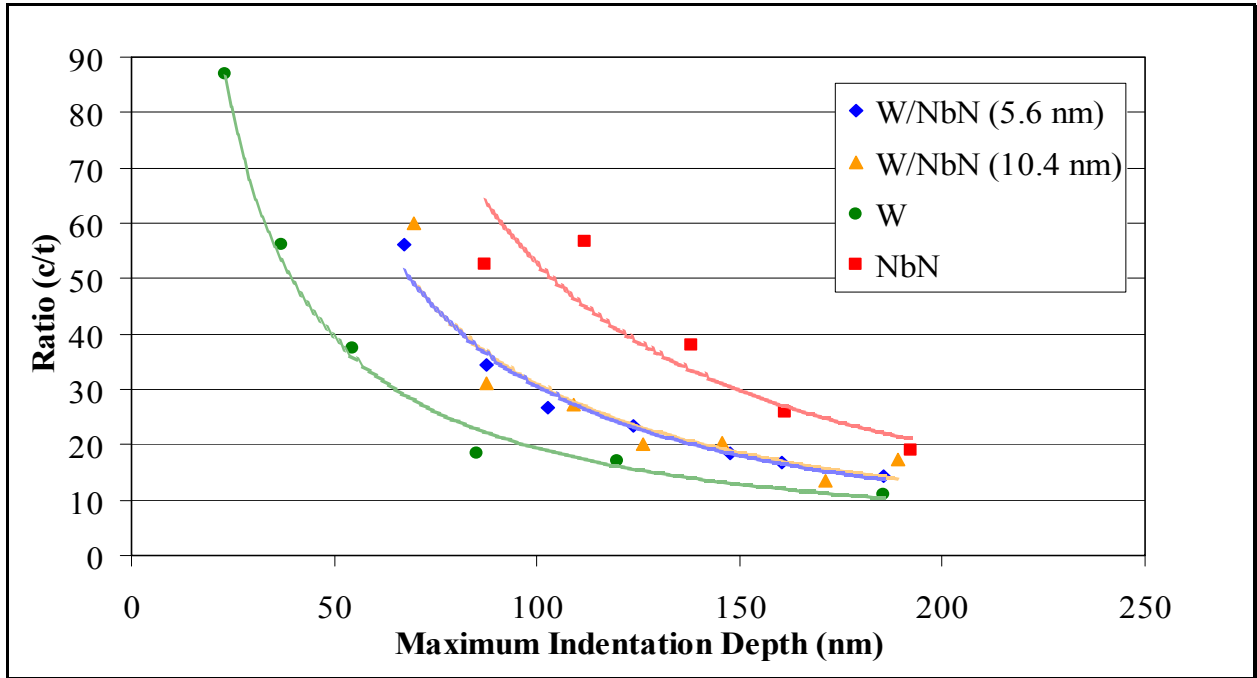


Figure 44: Ratio (c/t) as a function of maximum indentation depth, h_{\max} .

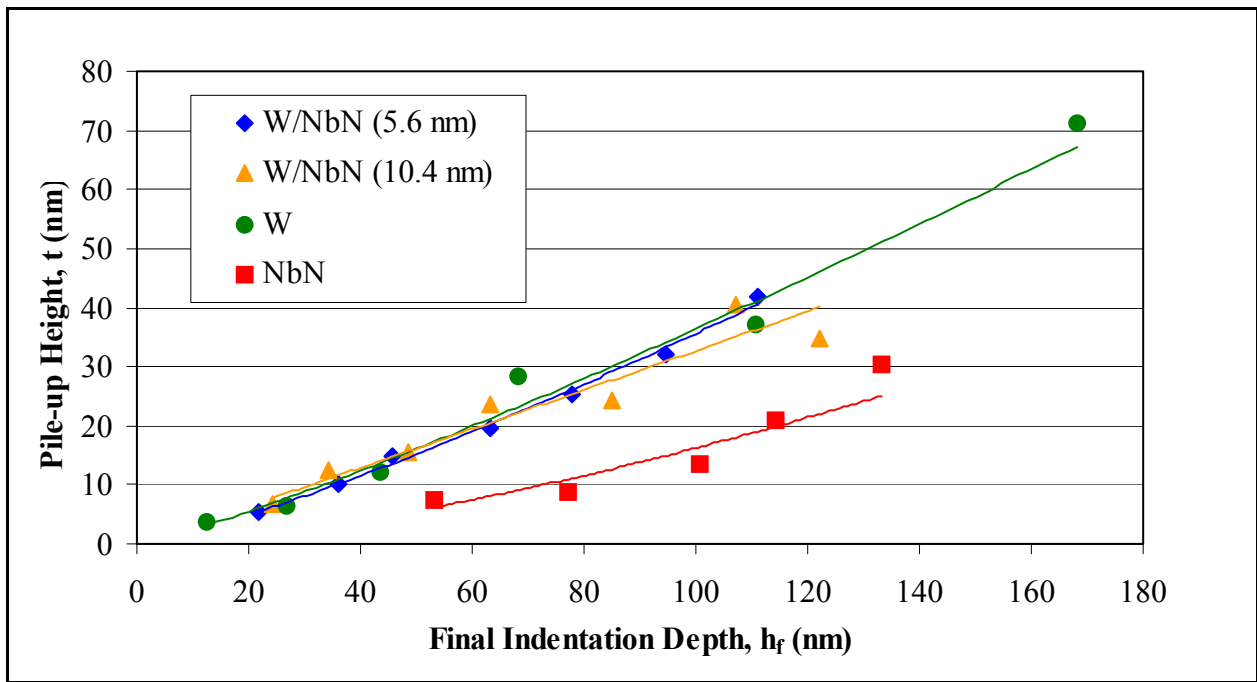


Figure 45: Pile-up Height, t , as a function of final indentation depth, h_f .

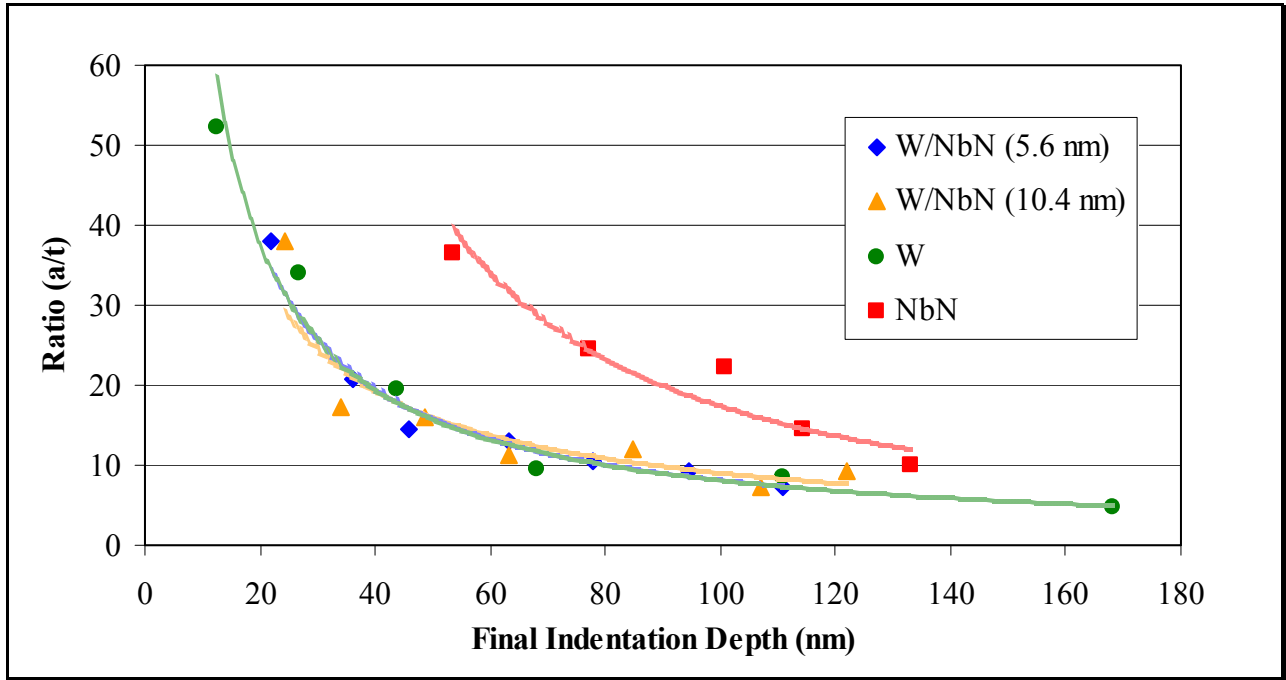


Figure 46: Ratio (a/t) as a function of final indentation depth, h_f .

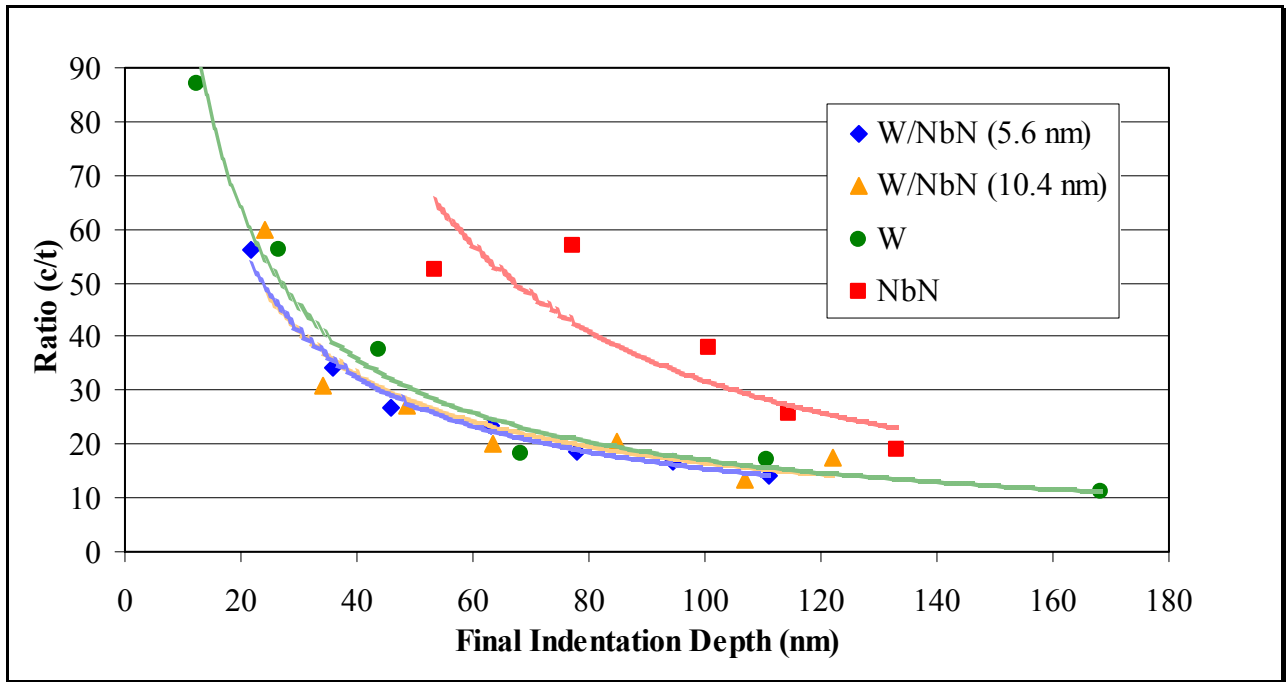


Figure 47: Ratio (c/t) as a function of final indentation depth, h_f .

As noted in the literature, the amount of pile-up in the indentation area is related to a variety of factors. While the indenter geometry is a factor, the characteristics of the material (such as Poisson's ratio, yield stress and the work hardening ability of the sample material) can also influence the amount of pile-up. [19, 20] Hence, it may be possible to draw some conclusions concerning the behavior of the materials by noting any trends in the curves. From Figures 42, 43 and 44, an examination of the parameters as a function of the *maximum* indentation depth shows that all four materials have similarly shaped curves. Furthermore, the curves for the two nanocomposites fall between the curves for the ceramic and metallic components. This is consistent with the behavior of normal composites where the composite response is expected to be somewhere between the behavior of its components. However, the graphs comparing the parameters as a function of the *final* indentation depth show a different pattern. In Figures 45, 46, & 47, the curves for the nanocomposites, W/NbN ($\Lambda=5.6$ nm) and W/NbN ($\Lambda=10.4$ nm), are the *same* as the curves for the metallic material, W. The ceramic material, NbN, still exhibits behavior different from the other materials. The above observations imply that the presence of the soft, ductile metal, W, in the superlattice material acts to alter the plastic deformation behavior of the ceramic, NbN, layer. Since the NbN layer is constrained between layers of W, the NbN layer in the superlattice materials is forced to a different deformation than when it is in its monolithic form resulting in the material pile-up observed for the two superlattice materials.

5.0 DISCUSSION

As noted at the outset, the hardness of the superlattice materials, W/NbN ($\Lambda=5.6$ nm) and W/NbN ($\Lambda=10.4$ nm), have been reported as 28 GPa and 26 GPa respectively. These values exceed not only the hardness of the individual materials, W (7 GPa) and NbN (17 GPa), comprising the nanocomposites, but also the hardness predicted by the rule of mixtures for composites. [1, 2] The objective of this investigation was to determine how to use the experimental data obtained from nanoindentations and image scanning to analyze this interesting behavior of the superlattice material in an effort to explain this discrepancy. In this section, the experimental results will be discussed to ascertain the influence that several factors may have on the hardness in the superlattice materials.

An examination of the hardness data shows the increase in the hardness observed in the superlattice materials at deeper indentation depths. However, the superlattice materials and NbN exhibit similar hardness at shallow indentation depths (i.e. less than 25 nm). This implies that the increase in hardness observed in the superlattice materials for the deeper indentations is due to the presence of the interface, since the influence of the interfaces would be minimal for shallow indentations due to the relatively small plastic deformation zone. Also, the similarity in hardness between the NbN sample and the two nanocomposites at the shallow indentation depths could be the result of a length scale effect occurring in the W layers. Since the individual layers are only a couple nanometers thick, the hardness of the W layer increases due to its confinement between the NbN layers. [21] Hence, the hardness for the superlattice materials at shallow indentations appears to be determined largely by the properties of the harder material in the nanocomposite.

The other mechanical property examined was the elastic moduli. It was noted that the reduced elastic moduli of the component materials are very similar to the reduced elastic moduli of the two superlattice materials. This implies that the *rate* of elastic recovery is not considerably altered in the two superlattice materials. Since the reduced moduli for all the samples are in the same approximate range, the influence of the elastic modulus on the hardness of the nanocomposites appears to be minimal. Consequently, it is not possible to attribute the increase in hardness observed in the superlattice materials to this particular material property.

The next set of experimental data examined were the load versus displacement curves. In general, the comparisons of these curves show that the superlattice materials require deeper penetration of the indenter tip to cause the same permanent deformation depth, h_f . Again, the shallow indentations showed little difference between the two superlattice material samples and the NbN sample. This is further evidence that the increase in hardness observed in the superlattice materials can be attributed to the presence of the interfaces between layers. The comparisons of the load versus displacement curves also indicated that would be advantageous to calculate the energy of indentation. From the comparisons of the total, elastic and plastic energies, it is evident that the presence of the interface influences the behavior of the nanocomposites in two ways: the total energy required to cause a given permanent deformation is increased and the relative contribution of the elastic energy to the total energy is greater than for either of the component materials.

The final set of data examined was the material pile-up surrounding the indentation site obtained from the post-indentation scanned images. The comparisons of the geometric parameters indicate that the material pile-up in the nanocomposites is the same as the material pile-up in the W sample when compared as a function of the final indentation depth. In contrast,

the NbN sample exhibits less material pile-up than the other materials. The smaller amount of material pile-up observed in the NbN sample is the result of the deformation process. For a ceramic material, the energy of indentation is absorbed by local cracking in the deformation zone under the indenter tip as depicted in Figure 48. Hence, little material pile-up occurs during indentation.

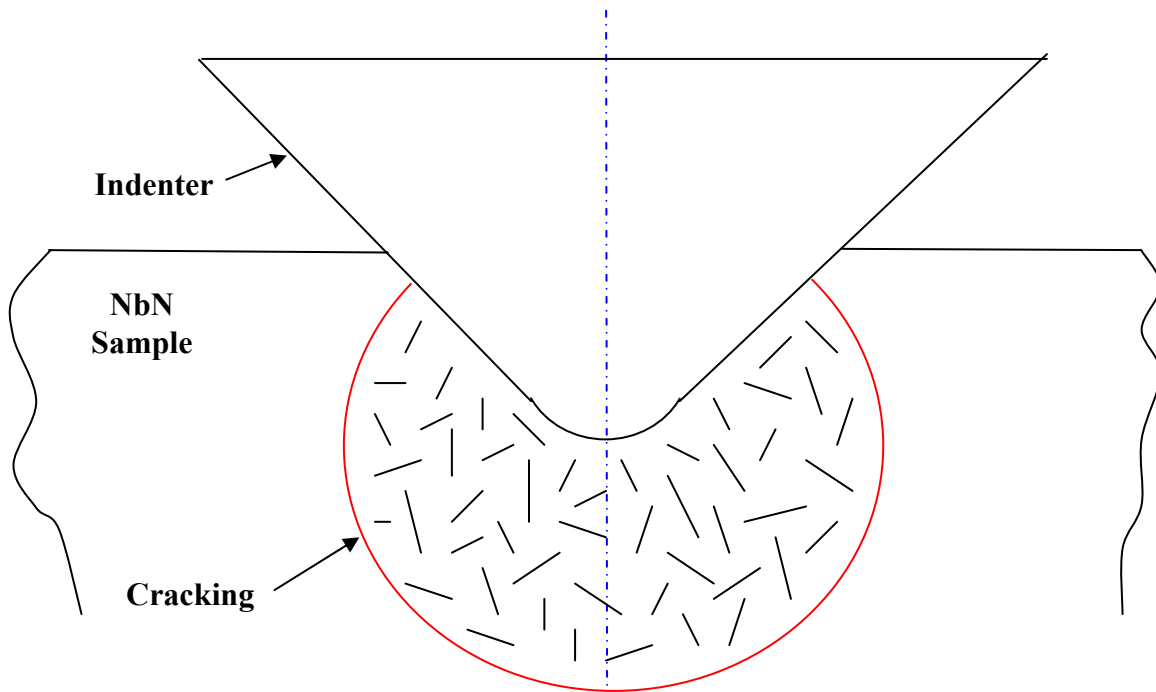


Figure 48: Cracking in the ceramic sample, NbN.

However, in the nanocomposites, the NbN layers surround the W layers. Due to the ductile properties of the W layers and the fact that the individual layers are only a few nanometers thick, the NbN layers are forced to bend with the W layers since the bending of the NbN layers is easier to achieve than fracture of the material. As a result, the presence of the W

layers act to alter the deformation process of the NbN layers from fracture to bending. The bending of the layers results in the material pile-up observed in the superlattice materials. This is illustrated in Figure 49.

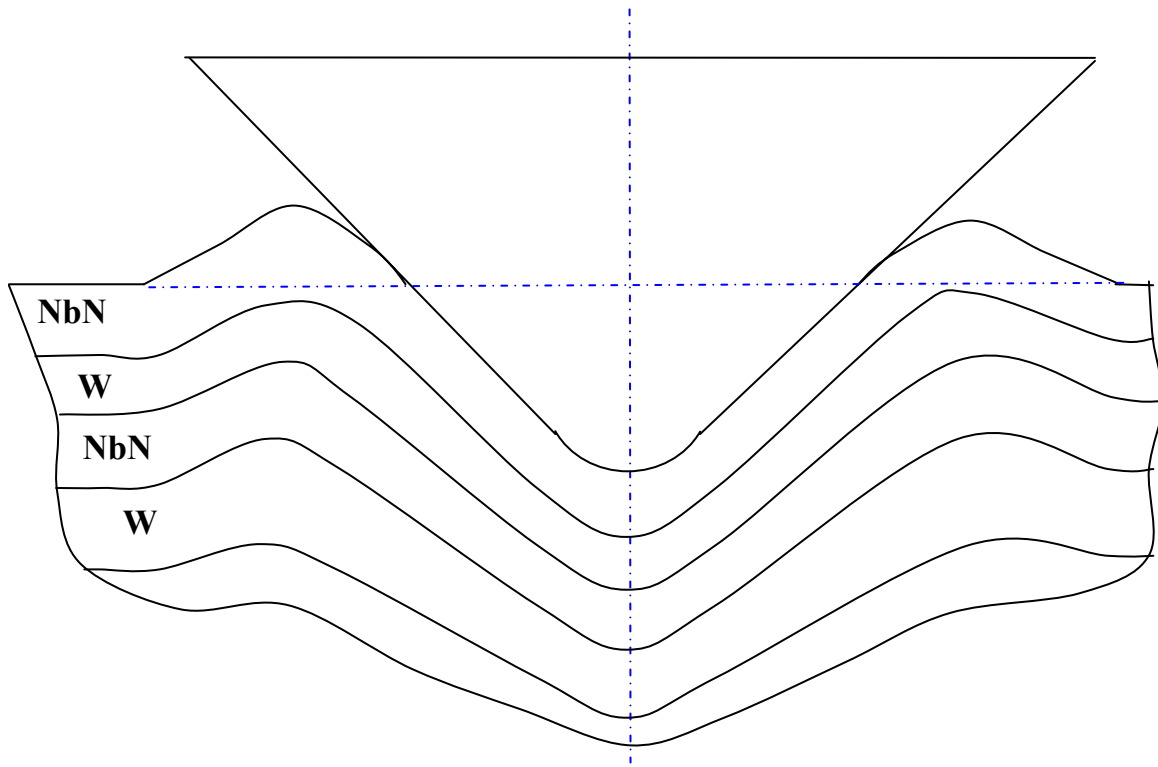


Figure 49: Bending of the nanolayers in the nanocomposites.

There is one final observation: although two samples of the superlattice material with different bilayer repeat periods were examined in this investigation, the difference in the behavior of the two superlattice material samples in the experimental results appears to be minimal. Therefore, in order to evaluate the influence of the layer thickness in greater detail, it would be necessary to examine samples with a greater difference in layer thickness.

6.0 CONCLUSIONS

The original objective of the investigation was to determine how to use the experimental data obtained from nanoindentations and image scanning to analyze the deformation behavior of a superlattice material. The mechanical properties were determined using the Oliver and Pharr method. [17] Comparisons of the hardness, the reduced elastic moduli, the load versus displacement curves, the energy of indentation and the material pile-up were made of two samples of the superlattice material W/NbN with different bilayer repeat periods ($\Lambda=5.6$ nm and $\Lambda=10.4$ nm) and the samples of the two monolithic materials constituting the nanocomposite. The results were discussed to evaluate the contributions of the different phenomenon to the increase in hardness observed in the superlattice materials. The following conclusions were made:

- (1) The shallow indentations show little difference in hardness between the NbN sample and the two superlattice materials. However, an increase in hardness is observed at deeper indentation depths. This indicates that the interface has a strong influence on the increase in hardness.
- (2) The observed increase in hardness is not related to the elastic modulus since the reduced elastic moduli for the NbN, W, W/NbN ($\Lambda=5.6$ nm) and W/NbN ($\Lambda=10.4$ nm) samples are in the same range.

- (3) More energy is required for indentation into the two nanocomposites to generate the same permanent deformation as in either component material.
- (4) Although super hardening exists in the nanocomposites, the deformation (i.e. pile-up) in the nanocomposites and the tungsten samples is greater than in the deformation in the ceramic material, NbN.

BIBLIOGRAPHY

BIBLIOGRAPHY

1. "Fundamentals of Nitride-Based Superlattice Thin Films". A. Madan and S. A. Barnett. From "Materials Science of Carbides, Nitrides and Borides", Y.G. Gogotsi and R.A. Andrievski (eds.), p. 187-204.
2. "Enhanced mechanical hardness in epitaxial non-isostructural Mo/NbN and W/NbN superlattices". A. Madan, Yun-yu Wang, S. A. Barnett, C. Engstrom, H. Ljungcrantz and L. Hultman and M. Grimsditch, *J. App. Phys.*, Vol. 84, No. 2, p. 776-785 (July 1998).
3. "Deposition, structure and hardness of polycrystalline transition-metal nitride superlattice films", X. Chu, M.S. Wong, W.D. Sproul, and S.A. Barnett, *J. Mater. Res.*, Vol. 14, No.6, p. 2500-2506 (Jun 1999).
4. "Structure and Strength of Multilayers", B. M. Clemens, H. Kung, and S. A. Barnett, *MRS Bulletin*, p.20-26, (Feb 1999).
5. "Dislocation-based deformation mechanisms in metallic nanolaminates", P.M. Anerson, T. Foecke and P.M. Hazzledine, *MRS Bulletin*, p.27-33, Feb (1999).
6. "Substrate effects on indentation plastic zone development in thin soft films", D. E. Kramer, A. A. Volinsky, N. R. Moody, and W.W. Gerberich, *J. Mater. Res.* Vol. 16, No.11, p. 3150-3157 (Nov 2001).
7. "Influence of thickness and substrate on the hardness and deformation of TiN films", M. Whitlting, A. Dendavid, P.J. Martin, and M. V. Swain, *Thin Solid Films* 270, p. 283-288 (1995).

8. "The Role of Plasticity in Bimaterial Fracture with Ductile Interlayers", N.I. Tymiak, A.A. Volinsky, M.D. Kriese, S.A. Downs and W.W. Gerberich, Metallurgical and Material Trans. A, Volume 31A, p. 863-872 (March 2000).
9. "Nanoindentation as a composition microprobe for nanolayer composites", M.F. Tambwe, D.S. Stone, J.-P. Hirvonen, I. Suni and S.-P. Hannula, Scripta Materialia, Vol. 37, No.9, p. 1421-1427 (1997).
10. "Between nanoindentation and scanning force microscopy: measuring mechanical properties in the nanometer regime", S. P. Baker, Thin Solid Films 308-309, p. 289-296 (1997).
11. "Elastic loading and elastoplastic unloading from nanometer level indentations for modulus determinations", W.W. Gerberich, W. Yu, D. Kramer, A. Strojny, D. Bahr, E. Lilleodeen, and J. Nelson, J. Mater. Res., Vol.13, No. 2, p. 421-439 (Feb 1998).
12. Private correspondence with Dr. Anita Madan, Northwestern University.
13. Samples fabricated by Dr. Anita Madan, Northwestern University.
14. "Mechanical properties of nanocomposite thin films", R. C. Cammarata, Thin Solid Films, 2450, p. 82-87 (1994).
15. "Elastic constants of single-crystal transition-metal nitride films measured by line-focus acoustic microscopy", J. O. Kim, J.D. Achenbach, P. B. Mirkarimi, M. Shinn and S. A. Barnett, J. App. Phys., Vol. 72, No. 5, p. 1805-1811 (Sept 1992).
16. SEM imaging of the indenter tip courtesy of Nicolas Perrusquia.
17. "An improved technique for determining hardness and elastic modulus using load and displacement sensing indentation experiments", W.C. Oliver and G.M. Pharr, J. Mater. Res., Vol. 7, No. 6, p. 1564-1583 (June 1992).
18. "Analysis of nanoindentation load-displacement loading curves", S. V. Hainesworth, H.W. Chandler, and T. F. Page, J. Mater. Res., Vol. 11, No. 8, p. 1987-1995 (Aug 1996).

19. "Plastic Zone and Pileup around Large Indentations", D.F. Bahr and W.W. Gerberich, *Met. and Mat. Trans. A*, Vol. 27A, p.3793-3800 (Dec 1996).
20. "Influences of pileup on the measurement of mechanical properties by load and depth sensing indentation techniques", A. Bolshakov and G.M. Pharr, *J. Mater. Res.*, Vol. 13, No. 4, p. 1049-1058 (April 1998).
21. "Length scale (thickness) controlled ductile versus brittle transition in layered materials", M.Z. Li and S.X. Mao, *Material Science and Engineering A266*, p. 73-79 (1999).